



HAL
open science

Combining spectroscopy and magnetism with geochemical tracers to improve the discrimination of sediment sources in a homogeneous subtropical catchment

Rafael Ramon, Olivier Evrard, J. Patrick Laceby, Laurent Caner, Alberto Inda, Cláudia A.P. De Barros, Jean P.G. Minella, Tales Tiecher

► To cite this version:

Rafael Ramon, Olivier Evrard, J. Patrick Laceby, Laurent Caner, Alberto Inda, et al.. Combining spectroscopy and magnetism with geochemical tracers to improve the discrimination of sediment sources in a homogeneous subtropical catchment. *CATENA*, 2020, 3535, pp.104800. 10.1016/j.catena.2020.104800 . cea-02908422

HAL Id: cea-02908422

<https://cea.hal.science/cea-02908422>

Submitted on 29 Jul 2020

HAL is a multi-disciplinary open access archive for the deposit and dissemination of scientific research documents, whether they are published or not. The documents may come from teaching and research institutions in France or abroad, or from public or private research centers.

L'archive ouverte pluridisciplinaire **HAL**, est destinée au dépôt et à la diffusion de documents scientifiques de niveau recherche, publiés ou non, émanant des établissements d'enseignement et de recherche français ou étrangers, des laboratoires publics ou privés.

1 **Combining spectroscopy and magnetism with geochemical tracers to improve the**
2 **discrimination of sediment sources in a homogeneous subtropical catchment**

3
4 Rafael Ramon^(a,b); Olivier Evrard^(b); J. Patrick Laceby^(c); Laurent Caner^(d), Alberto V.
5 Inda^(e), Cláudia A.P. de Barros^(e); Jean P.G. Minella^(f) and Tales Tiecher^(e)

6
7 ^a Graduate Program in Soil Science, Federal University of Rio Grande do Sul, Bento Gonçalves Ave.,
8 91540-000 Porto Alegre, RS, Brazil – Interdisciplinary Research Group On Environmental
9 Biogeochemistry - IRGEB (rafaramon11@gmail.com)

10 ^b Laboratoire des Sciences et de l'Environnement, UMR 8212 (CEA/CNRS/UVSQ), 91 191 Gif-sur-Yvette
11 Cedex (France), Université Paris-Saclay, France – IRGEB (olivier.evrard@lsce.ipsl.fr)

12 ^c Alberta Environment and Parks, 3535 Research Rd NW, T2L 2K8, Calgary, Alberta, Canada
13 (patrick.Laceby@gov.ab.ca)

14 ^d IC2MP-HydrASA UMR, Université de Poitiers, Poitiers, France (laurent.caner@univ-poitiers.fr)

15 ^e Department of Soil Science, Federal University of Rio Grande do Sul, Bento Gonçalves Ave. 7712,
16 91540-000 Porto Alegre, RS, Brazil – IRGEB (alberto.inda@ufrgs.br; claudia.barros@ufrgs.br;
17 tales.tiecher@gmail.com)

18 ^f Department of Soil Science, Federal University of Santa Maria, Roraima Ave. 1000, 97105-900 Santa
19 Maria, RS, Brazil – IRGEB (jminella@gmail.com)

22 **Abstract**

23 An important step in the sediment source fingerprinting approach is the selection of the
24 appropriate tracing parameters to maximize source discrimination. The use of multiple
25 tracing properties may reduce uncertainties and increase discrimination between
26 sources. Accordingly, this study investigates the discrimination and quantifies the
27 contribution of sediment sources delivering sediment to a river draining a
28 homogeneous subtropical agricultural catchment based on the combination of
29 ultraviolet-visible spectra derived parameters (UV), magnetic (M), and geochemical
30 tracers (GEO). The investigated catchment (Conceição River - 804 km²), located in
31 Southern Brazil, has predominantly deep and strongly weathered Ferralsols. The main
32 land-uses found in the area are cropland (89%), pasture (5%) and forest (5%). A total of
33 187 samples were collected to characterise the five main sediment sources, including
34 cropland, pastures, unpaved roads, gullies and stream banks. A total of 53 tracers,
35 including 21 geochemical tracers, two magnetic properties and 30 parameters derived
36 from UV spectra, were analysed. Tracers were selected following a three step
37 procedure, including: (i) an interquartile range test, (ii) a Kruskal–Wallis H test, and (iii)
38 a linear discriminant function analysis (LDA). The LDA was performed using six
39 different sets of variables: (i) GEO only; (ii) UV only; (iii) M+UV (MUV); (iv) GEO+UV
40 (GUV); (v) GEO + M (GM) and (vi) GEO+M+UV (GMUV). The selected tracers were
41 introduced into a mass balance mixing model to estimate the source contributions to in-
42 stream sediment by minimizing the sum of square residuals. Most geochemical tracers
43 were considered not conservative by using the interquartile range test in this catchment
44 with highly weathered soils. The GM approach resulted in the highest percentage of
45 samples correctly classified (SCC), with 74%, followed by the approaches with GMUV
46 and GUV, with 73%. Alternative tracers, UV individually or combined with M tracers,

47 correctly classified only 59 and 60% of the samples, respectively. Moreover, they did
48 not provide significant additional discrimination power even when combined with the
49 GEO tracers. The apportionment model resulted in similar source contribution results
50 for all approaches, with the absence of significant difference when comparing the mean
51 source contributions obtained for the entire set of sediment samples (Cropland: 17–
52 23%; Pastures: 24–34%; Unpaved Roads: 3–12%; Stream Banks: 26–31%; Gullies: 14–
53 19%). Due to the strong homogeneity of soil types found in the Conceição catchment,
54 these differences in source contributions remained very low and the results of the
55 mixing model were impacted by the high number of potential sources and the relatively
56 limited quality of the sediment source discrimination. According to the model results,
57 the low discrimination between the potential sediment sources illustrates the
58 difficulties for discriminating land-used based sediment sources, with more than three
59 potential sources, in homogeneous catchments with highly weathered soils (e.g.
60 Ferralsols, Nitisols) under tropical conditions.

61

62 **Highlights**

63 Geochemical tracers were not conservative in a catchment with highly weathered soils.

64 Magnetic and UV tracers had low discriminating potential between land uses.

65 The low discrimination between sources results in great uncertainties in the results.

66 Quantifying sediment contributions from more than three sources remains challenging.

67 Despite limited discrimination, results of all tracers combinations remained consistent.

68

69 **Key Words**

70 Sediment fingerprinting; soil erosion; composite fingerprinting, tracer selection,

71 geochemistry.

72

73

74 **1 Introduction**

75 The sustainable production of food, fiber and fuel remains limited by soil
76 erosion. Despite the vast knowledge accumulated about soil erosion, it remains a
77 significant global environmental issue that is one of the main causes of soil degradation
78 worldwide. In this context, Southern Brazil has one of the highest erosion rates in the
79 world (Borrelli et al., 2017) due to the relief characteristics along with intense and
80 erosive rainfall (Ramon et al. 2017). In particular, rainfall erosivity is expected to
81 increase ~10% in Southern Brazil by 2040 (Almagro et al., 2017).

82 Although field research programs are an essential tool to understand the impacts
83 of human activities and climate changes on natural resources (Poesen, 2017), in Brazil
84 they have been employed only relatively recently compared to other regions of the
85 world such as the United States or Europe (Melo et al., 2020). In this scenario of limited
86 hydrological and geomorphological understanding, it is important to identify the main
87 sediment sources (Collins et.al, 2017) to guide decision-makers in the efficient
88 allocation of limited public resources available to mitigate soil erosion and sediment
89 production.

90 The sediment fingerprinting technique has been increasingly used in catchments
91 worldwide to quantify the relative source contributions to river sediment (Walling,
92 2013). The method offers an effective way to calculate the contribution of diffuse
93 sources of sediment and contaminants, providing useful information to focus efforts on
94 controlling major soil erosion problems (Niu et al., 2019; Nosrati and Collins, 2019;
95 Torres Astorga et al., 2018; Uber et al., 2019). However, many challenges require
96 further research with sediment source fingerprinting such as the selection of tracers to

97 analyse and the grouping of the main sediment sources (Pulley et al., 2017b; Smith et al.,
98 2015).

99 Sediment tracer properties need to be conservative and their signature from
100 source to the river network must remain constant or vary predictably (Belmont et al.,
101 2014; Laceby et al., 2017). Although it is known that the conservativeness of potential
102 inorganic tracers is dependent on their chemical nature (e.g., alkali metals, transition
103 metals, rare earth elements) and how they are bound to the sediment (e.g., sorbed onto
104 sediment particles or matrix-bounded elements), there is still no consensus on the best
105 approach to assess conservativeness.

106 Most studies typically evaluate conservativeness empirically through
107 comparisons of concentration between sources and sediments, which in turns depend
108 on the conservativeness test applied (Smith et al., 2018; Lizaga et al., 2020). Moreover,
109 tracer conservativeness can also be dependent on the characteristics of the studied
110 catchment and the sediment sources evaluated. Studying land use sources in
111 homogeneous catchments may be much more challenging as any enrichment or
112 depletion of a particular element during the erosion process can result in sediment
113 concentrations varying outside the range of source values (Smith and Blake, 2014). To
114 overcome conservativeness issues and increase the number of conservative tracers,
115 physical characteristics such as colour, or related to mineralogical constitution, such as
116 magnetism and parameters related to Fe oxides, that can be easily measured, may
117 potentially maintain their conservativeness in these homogeneous catchments and be
118 combined with other tracing parameters (Pulley et al., 2018).

119 In addition, tracer properties should ideally be low-cost, quick and easy to
120 analyse, as characterizing a large number of samples is needed in order to be
121 representative of the within-source variability, especially in large catchments.

122 Furthermore, analyses that require a low sample mass and are non-destructive are
123 preferable, as in several environmental contexts, it can be difficult to collect large
124 quantities of suspended sediment during fieldwork (Guzmán et al., 2013).

125 Geochemical composition of source and sediment samples is among the most
126 used tracers for sediment fingerprinting worldwide (Koiter et al., 2013). Multiple
127 geochemical analyses such as inductively coupled plasma (ICP) or X-ray fluorescence
128 analyses result in high number of potential tracers, however they are not an option for
129 research groups that do not have access to sophisticated equipment (e.g. ICP-OES or
130 ICP-MS, microwave oven) or sufficient resources to afford such analysis.

131 Another option for tracing sediment sources are magnetic properties which have
132 been widely used since the original sediment fingerprinting studies (Walling et al.,
133 1979; Yu and Oldfield, 1989). Some measures like magnetic susceptibility can be easily
134 measured with relatively basic equipment (Rowntree et al., 2017), increasing the
135 number of tracers available for multiple sources contribution apportionment.

136 Moreover, spectroscopy data have been intensively investigated in the last
137 decade as a low-cost, non-destructive and straightforward alternative method to
138 provide tracer properties (Poulenard et al, 2009; Pulley et al., 2018). A variety of
139 approaches have been used to incorporate spectroscopy analysis into sediment
140 fingerprinting research (Legout et al., 2013; Martínez-Carreras et al., 2010b; Poulenard
141 et al., 2012; Tiecher et al., 2017). Among them, the use of colour parameters and
142 spectral features derived from ultraviolet-visible (UV) has shown to be promising
143 because it can be used alone or incorporated into mathematical models together with
144 geochemical tracers, radionuclides and others (Brosinsky et al., 2014a, 2014b, Tiecher
145 et al., 2015). Ultra-violet derived parameters may therefore offer a strong potential for

146 sediment tracing, although the proper classification of sources and the use of effective
147 modelling strategies are required to obtain reliable results (Pulley et al., 2018).

148 An important question in sediment fingerprinting surrounds the proper
149 identification of the potential sources of sediment to be incorporated into end-member
150 mixing models. Reducing the number of sources considered based on their relevance in
151 the study sites, or regrouping similar sources is a common practice in sediment
152 fingerprinting studies. For instance, Pulley et al. (2015b) did not consider grassland as a
153 source, since it occupied only a very low proportion of the catchment area and because
154 it was not possible to discriminate between cultivated and grassland areas with the
155 tracers used. A similar decision was taken by Minella et al. (2004), where fallow areas
156 could not be distinguished from pasture by the geochemical tracers used, and then they
157 were combined, while channel banks and new fields were removed because there was
158 not enough data to discriminate them, reducing the previous six sources to three.

159 In a previous study conducted in the Conceição River catchment in Southern
160 Brazil, pastures were not considered as potential sources, since the geochemical tracers
161 were not able to discriminate pastures from croplands and because they occupy only a
162 low percentage of the total catchment surface area (Tiecher et al., 2018). Gullies were
163 also not considered, as they are not commonly observed in the Conceição catchment,
164 where rill erosion is much more widespread (Didoné et al., 2015). In this catchment,
165 which consists of relatively homogeneous soil and geology, geochemical tracers were
166 only able to correctly classify only 84% of the samples in their respective source groups
167 (ie., cultivated sources, unpaved roads and streambanks) (Tiecher et al., 2018). The
168 small difference in the elemental concentrations observed between the sources, because
169 of intense weathering and leaching of most elements except Al and Fe, complicated their

170 discrimination, requiring further studies and alternative tracers to increase the
171 robustness of the results.

172 Here, the use of low-cost alternative parameters, including spectroscopy
173 derivatives in the ultraviolet-visible range and magnetic parameters, in combination
174 with geochemical tracers are investigated to provide an alternative approach that
175 increases the discrimination between multiple land use sources. This research
176 investigates the potential of six different sets of tracing parameters combining low cost
177 and geochemical element traces to calculate the respective contributions of five
178 potential sediment sources in a homogeneous catchment (Conceição River) in southern
179 Brazil. This research contributes to the ongoing development of low-cost tracers,
180 examining their efficacy in a complicated homogeneous tracing environment, that is
181 representative of regions with extensive agricultural activities that contribute
182 deleterious sediment loads degrading waterways worldwide.

183

184 **2 Methodology**

185 **2.1 Study site**

186 The Conceição River catchment is located on a basaltic plateau in the southern
187 part of the Paraná Basin in the state of Rio Grande do Sul, and it covers an area of
188 approximately 804 km² (Figure 1). According to Köppen's classification, the climate is
189 classified as of Cfa type, humid subtropical without a defined dry season, with an
190 average annual precipitation ranging between 1750 to 2000 mm per year and an
191 average temperature of 18.6°C. This catchment is representative of the basaltic plateau
192 region of the Serra Geral Formation (92%), where the soil classes found are Ferralsols
193 (80%), Nitisols (18%) and Acrisols (2%), with a mineralogy dominated by iron oxides

194 and kaolinite (Figure 2). These soils are very rich in clays, typically, the Ferralsols that
195 predominate in this catchment have less than 10% of sand and clay content as high as
196 85% (Ramos et al., 2017). Small areas from the Tupanciretã Formation (6%), which are
197 outcrops of the Botucatu Formation enclosed by volcanic spills of the Serra Geral
198 Formation, are also found. The relief of the catchment is characterized by gentle slopes
199 (6-9%) at the higher positions of the landscape and steeper slopes (10-14%) near the
200 drainage channels, with altitudes ranging from 270 to 480 m a.s.l. The catchment outlet
201 is located next to the monitoring point number 75200000 of the National Water Agency
202 (ANA) (28°27'22" S, 53°58'24" O) in the municipality of Ijuí.

203 The main land use is cropland (89%) mainly cultivated with soybean (*Glycine*
204 *max*) under no tillage system in the summer and with wheat (*Triticum aestivum*) for
205 grain production, oat (*Avena sativa* and *Avena strigosa*) and ryegrass (*Lolium*
206 *multiflorum*) for dairy cattle feed or used as cover crops for protecting the soils during
207 winter. However, inadequate soil management in these areas, without crop rotation,
208 cover crops during the autumn and winter, and mechanical practices to control surface
209 runoff, has resulted in high erosion rates during the last 60 years, even with the no-
210 tillage system implemented during the last 30 years (Didoné et al., 2019, 2015).
211 Grasslands and pasture, mainly used for cattle raising, cover 5% of the total surface
212 area, whereas forest is found on only 5% of the surface. Approximately 1 to 2% of the
213 area is occupied by non-vegetated areas, urban infrastructure and water bodies.

214 2.2 Source and sediment sampling

215 Soil composite samples (n=187) were collected in areas representative of the
216 potential sediment sources, which include cropland (n=77), pasture (which include
217 grasslands and permanent pastures, n=24), unpaved road (n=38), stream bank (n=34)
218 and gullies (n=14) (Figure 2). The source samples were taken from the surface layer (0

219 – 5 cm) of cropland and pasture (surface sources). In gully sites and stream bank
220 samples were taken from the exposed sidewall avoiding the material of the most
221 superficial layer (0-5 cm). The height exposed in the gullies sites and stream banks
222 varies greatly, but as the soil below the surface layer is quite homogeneous in the
223 Ferralsols of this catchment, the samples were collected in a representative manner
224 throughout the exposed subsurface area. To characterize unpaved roads, samples were
225 taken mainly in the roadsides where erosion is more evident, which in all cases
226 correspond to the subsurface of the soil, always avoiding collecting transient materials
227 from other potential sources. Care was taken to avoid those sites that have accumulated
228 sediment originating from other sources. Around ten sub-samples were collected within
229 a radius of approximately 50 m and mixed to prepare a composite sample, in order to
230 obtain representative source material. Samples were taken at sites sensitive to erosion
231 and connected to the stream network, and attention was paid to cover all the range of
232 soil types found in the catchment.

233 Eleven sediment samples were collected at the catchment outlet during the
234 monitoring period (Appendix A). From these, eight samples are fine-bed sediment (FBS)
235 collected in the bottom of the river with a suction device and three samples were
236 collected with a time-integrated sediment sampler (TISS) designed according to Phillips
237 et al. (2000). The period during which the TISS was sampled and the collection date of
238 each FBS sample are detailed in Table 1.

239 2.3 Source and sediment analyses

240 All samples were oven-dried (50°C), gently disaggregated using a pestle and
241 mortar and dry-sieved to 63 µm to avoid particle size effects prior to further analysis
242 (Koiter et al., 2013; Laceby et al., 2017).

243 2.3.1 Geochemical properties

244 A total of 20 geochemical elements were evaluated as potential tracers. The total
245 concentration of Al, Ba, Be, Ca, Co, Cr, Cu, Fe, K, La, Li, Mg, Mn, Na, Ni, P, Sr, Ti, V, and Zn
246 was determined using inductively coupled plasma optical emission spectrometry (ICP-
247 OES) after microwave-assisted digestion with concentrated HCl and HNO₃ (ratio 3:1) for
248 9.5 min at 182 °C. This method was adapted from U.S. EPA (2007), as it was reported to
249 provide satisfactory recovery for quantifying metal concentrations in soils (Chen and
250 Ma, 2001; Da Silva et al., 2014). Total organic carbon (TOC), which was estimated by
251 wet oxidation (K₂Cr₂O₇ + H₂SO₄ - Walkley and Black, 1934), was included in the set of
252 geochemical tracers.

253 2.3.2 Magnetic properties

254 Two grams of each sample were used to measure the magnetic susceptibility in a
255 Bartington MS2B Dual Frequency sensor, with three readings for each sample at high
256 (4.7 kHz) and low frequencies (0.47 kHz) to obtain the mass specific magnetic
257 susceptibility for high ($\chi_{HF} - m^3 kg^{-1}$) and low frequencies ($\chi_{LF} - m^3 kg^{-1}$) (Mullins,
258 1977).

259 2.3.3 Ultraviolet-visible analysis and parameters calculation

260 The diffuse reflectance spectra in the ultraviolet-visible (UV) wavelengths (200
261 to 800 nm, with 1 nm step) were measured for each powdered sample using a Cary
262 5000 UV-NIR spectrophotometer (Varian, Palo Alto, CA, USA) at room temperature,
263 using BaSO₄ as 100% reflectance standard. Twenty-two colour parameters were
264 derived from the UV spectra following the colorimetric models described in details by
265 Viscarra Rossel et al. (2006), which are based on the Munsell HVC, RGB, the
266 decorrelation of RGB data, CIELAB and CIELUV Cartesian coordinate systems, three
267 parameters from the HunterLab colour space model (HunterLab, 2015) and two indices

268 (coloration – CI and saturation index – SI) (Pulley et al., 2018). In total, 27 colour metric
269 parameters were derived from the spectra of source and sediment samples (L, L*, a, a*,
270 b, b*, C*, h, RI, x, y, z, u*, v*, u', v', Hvc, hVc, hvC, R, G, B, HRGB, IRGB, SRGB, CI and SI).
271 Three other parameters were calculated from the second derivative curves of remission
272 functions in the visible range of soil and sediment samples, which displayed three major
273 absorption bands at short wavelengths commonly assigned to Fe-oxides (Caner et al.,
274 2011; Fritsch et al., 2005; Kosmas et al., 1984; Scheinost et al., 1998) (Appendix B).

275 2.4 Sediment source discrimination and apportionment

276 The selection of the discriminant tracers followed the classical three-step
277 procedure, including: i) a range test; ii) the Kruskal-Wallis H test (KW H test); and iii) a
278 linear discriminant function analysis (LDA) (Collins et al., 2010a). In the range test,
279 variables with median \pm the interquartile range (IQR, 25th and 75th percentiles) values
280 of sediment samples lying outside the range of the sources were excluded (Batista et al.,
281 2018). The KW H test was performed to test the null hypothesis ($p < 0.05$) that the
282 sources belong to the same population. The variables that provided significant
283 discrimination between sources were analysed with a forward stepwise LDA ($p < 0.1$) in
284 order to reduce the number of variables to a minimum that maximizes source
285 discrimination (Collins et al., 2010b). The statistical analyses were performed with R
286 software (R Development Core Team, 2017) and more details can be found in Batista et
287 al. (2018).

288 The source contributions were estimated by minimizing the sum of squared
289 residuals (SSR) of the mass balance un-mixing model. Optimization constraints were set
290 to ensure that source contributions were non-negative and that their sum equalled 1.
291 The un-mixing model was solved by a Monte Carlo simulation with 2500 iterations.
292 More information about model settings and compilation can be found in Batista et al.

293 (2018). Model uncertainties were evaluated based on the interquartile variation range
294 of the predictions from the multiple interactions of the Monte Carlo simulation. The
295 standard deviation (SD) of the Monte Carlo simulation results is calculated for each
296 sediment sample and source.

297 In order to test the ability of magnetic (M) and ultraviolet-visible derived
298 variables (UV) to discriminate between sediment sources, six approaches were tested to
299 verify the contribution of each variable dataset. A first approach was carried out
300 considering only geochemical variables (GEO) as potential tracers and the LDA and
301 apportionment model results were compared to those obtained with geochemical
302 tracers combined with M variables (GM), GEO plus UV (GUV), all variables together
303 (GMUV) and UV variables alone. Finally, an approach was carried out considering only
304 those “alternative” variables, involving M plus UV derived parameters (MUV).

305 **3 Results**

306 **3.1 Selection of sediment tracers**

307 All parameters were analysed individually to check their conservative behaviour
308 and the property distribution in each group was evaluated using box plots. The
309 interquartile range was more restrictive than the classical range test based on
310 maximum and minimum values measured in the sources, resulting in a high number of
311 tracers (70 %) removed by the range test (Table 2). From the 21 geochemical elements,
312 only five behave conservatively (TOC, Be, Fe, K and P) . The set of 30 UV parameters
313 included nine conservative properties (L^* , x , L , a , b , v^* , v' , hVc , and B). Magnetic
314 parameters, \square_{HF} and \square_{LF} were both conservative. It means that about 24, 30 and 100%
315 of geochemical, UV parameters and magnetism tracers, respectively, behaved
316 conservatively when applied the IQR range test. If applied the classical range test, about

317 72, 97 and 100% of geochemical, UV parameters and magnetic tracers, respectively,
318 behaved conservatively.

319 The KW H test was applied to all tracers, even to those that were not retained by
320 the conservativity test. Only five tracers did not hold potential to discriminate between
321 at least two potential sources (Cu, Ni, Fe, Na and A2 had $p > 0.1$) (Table 4). Among the
322 parameters that were conservative and passed the KW H test, the combination of
323 tracers that best discriminated between the sources was selected by the LDA, which are
324 presented in Table 3.

325 When geochemical data were used as potential tracers, P, K and TOC were
326 always selected as tracers. TOC and P are well correlated (Figure 3) and they have a
327 higher concentration in the surface samples (24 g kg⁻¹ and 445 mg kg⁻¹) than in the
328 subsurface samples (11 g kg⁻¹ and 300 mg kg⁻¹). The mean concentration of TOC and P
329 found in the sediment (22 g kg⁻¹ and 468 mg kg⁻¹) was close to that observed in the
330 surface sources. K had no correlation with P and TOC, besides having higher
331 concentrations in the surface sources (875 mg kg⁻¹). The K concentration in the
332 sediments varied widely, with a standard deviation closer to the mean (397 ± 362 mg
333 kg⁻¹), which makes this value similar to that found in subsurface sources (565 mg kg⁻¹).
334 Potassium and P presented higher concentrations in the cropland samples due to the
335 addition of fertilizers for crop production. TOC presents higher concentrations in the
336 pastures, which can be attributed to the permanent soil cover and the increase of
337 below-ground biomass induced by well managed animal grazing (López-Mársico et al.,
338 2015; Schuman et al., 1999; Tornquist et al., 2009). Iron was considered as conservative
339 although it did not provide discrimination between sediment sources. This was
340 somehow expected, since highly weathered soils have a high content of Fe oxides across
341 the entire soil profile, making comparison of surface and subsurface sources very

342 difficult. Beryllium was conservative, but its variation between sources was very low,
343 presenting low potential for discrimination between sources (KW *H* test $p > 0.01$).
344 Finally, the LDA selected only P, K and TOC as tracers for the GEO approach, which did
345 not comply with the universal rule of the discriminant analysis for multiple groups,
346 stating that the number of tracers must be at least equivalent to the number of groups
347 (n) minus one ($n-1$) (Rencher, 2005). For this reason, the use of geochemical tracers
348 alone was not modelled.

349 In the approach using GEO and M parameters (GM), the LDA selected two
350 magnetic parameters (χ_{LF} , χ_{HF}) and the three previously selected geochemical
351 elements. The two M parameters were highly correlated (Figure 3) and they remained
352 in the same cluster group of tracers, although they differed completely from the group
353 of the other three geochemical elements (Figure 4). Therefore, the LDA kept the two M
354 parameters, which improved the discrimination of the sources, resulting in 74.3% of
355 SCC. The differences of magnetic susceptibility values between sources for the two
356 magnetic parameters, χ_{LF} and χ_{HF} , are similar, where unpaved roads presented higher
357 values (22×10^{-6} and $19 \times 10^{-6} \text{ m}^3 \text{ kg}^{-1}$, respectively), followed by croplands, pastures,
358 gullies and stream banks (Table 4). Sediment samples have magnetic susceptibility
359 values (14×10^{-6} and $13 \times 10^{-6} \text{ m}^3 \text{ kg}^{-1}$, respectively) closer to those observed for
360 pastures (15×10^{-6} and $14 \times 10^{-6} \text{ m}^3 \text{ kg}^{-1}$, respectively) and stream banks (11×10^{-6} and
361 $10 \times 10^{-6} \text{ m}^3 \text{ kg}^{-1}$, respectively).

362 The same parameters were selected for the combination of GEO and UV
363 parameters (GUV) and the combination of GEO, UV and M parameters (GMUV). For the
364 UV parameters, a , v^* , b , L and L^* were selected by the LDA, increasing the SCC to 73.3%,
365 an increase of 4.9% compared to the use of GEO tracers alone. The parameter L and L^*
366 are related to the variation between white and black colours, also considered as the

367 luminosity index from HunterLab and CIELAB, respectively. Stream banks, gullies and
368 unpaved roads, which are subsurface sources (mean of 34 and 41 for L and L*,
369 respectively), had the highest values, which means that they have lighter colours than
370 the surface sources (mean of 32 and 39 for L and L*, respectively). L and L* mean values
371 for sediment samples (31 and 37, respectively) were lower than for all sources and
372 closer to those found in surface sources. More positive values for *a* and *b* means that the
373 colour is more red and yellow, respectively. Subsurface sources tend to be more red and
374 yellow, as *a* and *b* values are higher in this material (13.9 and 13.5, respectively) than in
375 surface sources (11.7 and 12.0, respectively). The mean values for sediments (9.0 and
376 11.4, respectively) were very close to those of the surface sources. The same behaviour
377 was observed for the parameter v^* (21.3 and 23.9 for surface and subsurface sources,
378 respectively), which is the CIELUV colour space model derived parameter equivalent to
379 the *a* from CIELAB.

380 When UV parameters were used individually, the percentage of SCC was the
381 lowest among all the tested tracer combinations, with 59.4% of SCC. The UV parameters
382 selected in this approach were *a*, v^* , v' and *b*. Besides the other parameters selected in
383 the other approaches, the parameter v' was selected in the UV approach, which is
384 related to the chromacity coordinates u^* and v^* from the CIELUV model. When the UV
385 and M parameters were combined, two M parameters were selected, but it did not
386 improve the source classification by the DFA, increasing only by 1% the proportion of
387 SCC. The reclassification of source samples by the LDA using the tracers selected in each
388 approach is illustrated in the bi-plot graphs (Figure 5a, 6a, 7a and 8a).

389

390 3.2 Model results for each approach

391 According to the five approaches modelled (UV, MUV, GUV, GM and GMUV), not
392 including the GEO only model as it had insufficient tracers for the number of sources,
393 pasture had the highest sediment contribution for most approaches, except when
394 geochemical tracers were combined with magnetic tracers, supplying sediment
395 proportions ranging from 24 to 33%. Stream bank and cropland were the second and
396 third sources in increasing order of contribution, with contributions ranging from 26 to
397 31% and 17 to 23%, respectively. Gullies were the fourth contributing source, with a
398 sediment delivery proportion varying between 16 and 19%. Unpaved roads provided
399 the lowest contribution to the river sediment, ranging from 2.6 to 12.2%. The mean
400 relative contributions of each source did not vary significantly between approaches
401 when the mean contributions for all sediment samples are compared, with the
402 exception of unpaved roads, for which the UV approach led to different results (Table
403 5).

404 When sediment samples were separated according to the sampling strategy,
405 significant differences between approaches were observed for cropland and unpaved
406 roads for both sampling strategies (Table 5). Comparing the type of sediment samples,
407 cropland had a higher contribution to TISS samples (16 to 39%) compared to FBS
408 samples (15 to 25%). The contribution of pastures to TISS samples was even higher,
409 ranging from 32 to 40%. Unpaved roads had a larger contribution to FBS samples
410 (~10.5%) and contributed less to the TISS samples (~3.5%). For pasture and stream
411 bank, significant differences between approaches were observed for FBS (19.9 to
412 33.2%) and TISS (16.8 to 31.8%) samples, respectively, while for gullies no difference
413 was observed for any sampling strategy.

414 The differences in sediment source contributions are mainly observed between
415 the approaches with only alternative tracers (UV and MUV) to those with geochemical
416 parameters included. Figure 5b to 8b provide box plots demonstrating the variation in
417 mean source contributions for all sediment samples when taking into account the 2500
418 Monte Carlo interactions results obtained for each approach. The large variations in
419 source contributions obtained for each set of simulations resulted in a standard
420 deviation (SD) that varied between 19 and 34% depending on the source considered
421 (Table 5).

422 The sediment source contributions predicted by the five approaches were
423 similar for the samples collected following the FBS sampling strategy, while the
424 variation between approaches was higher for the TISS samples (Figure 9). Pasture
425 provided the main source of TISS samples according to all approaches, contributing
426 more than 32% of sediment, followed by cropland with more than 24%, with the
427 exception of the approaches based on UV and MUV parameters, according to which
428 cropland contributed only 16 and 18% of sediment, respectively. For the FBS samples,
429 stream bank provided the main source of sediment, contributing more than 25% of the
430 material delivered to the river, with the exception of the approaches based on UV and
431 MUV parameters, according to which pasture was the main source of sediment, with 33
432 and 31%, respectively.

433

434 **4 Discussion**

435 4.1 Tracer selection and discrimination between sources

436 The conservative behaviour of a sediment property may vary according to
437 different factors (e.g. physical, biochemical and geochemical), requiring an appropriate

438 selection of those that do not suffer modifications from their sources to the sediment
439 sampling site, avoiding uncertainties in the sediment fingerprinting technique (Koiter et
440 al., 2013; Sherriff et al., 2015). There are different strategies to verify that a certain
441 tracer is conservative or not, such as the commonly used range test (Navratil et al.,
442 2012; Palazón and Navas, 2017a; Smith and Blake, 2014), where the value of a given
443 tracer measured in sediment must lie within the range of values observed in the
444 sources. However, the statistical test chosen can select different tracers and,
445 consequently, lead the final mixing model to provide different results (Gaspar et al.,
446 2019). In addition, the conservatism test based on mathematical and statistical tests
447 only cannot confirm that the tracer behaves conservatively (Collins et al., 2017b).

448 In the current research, the classical range test based on the maximum and
449 minimum values found in the source samples indicated that 87% of the total variables
450 were conservative, while with the IQR test, only 30% were considered to be
451 conservative. The range test based on maximum and minimum values observed in the
452 sources is less restrictive because, with this test, having only one extreme value for a
453 source sample is sufficient to make the range wider. At the same time, if only one
454 sediment sample has a value outside of the range, it is sufficient to remove the
455 parameter from further analysis. This situation was observed for K and TOC, which
456 were not retained after applying the minimum/maximum range test, because K was not
457 detected in two sediment samples and TOC had a higher concentration in one sediment
458 sample than in the sources, removing two of the three commonly best geochemical
459 tracers used to discriminate potential sediment sources in agricultural catchments. The
460 range test based on IQR proposed by Batista et al. (2018) provided more reasonable
461 results, as it kept only those tracers for which the values measured in the target samples
462 lied within the range found in the sources. Accordingly, it allowed keeping parameters

463 that would have been removed otherwise because only one sediment sample was
464 outside of the range of values measured in the sources. Future research considering the
465 application of alternative conservativeness tests for this homogeneous catchment, such
466 as bi-plots or more complex methods considering organic carbon and particle size
467 dependency, may help to select the most appropriate tracers (Smith et al., 2018; Lizaga
468 et al., 2020).

469 The potential of multiple sets of tracers to improve the discrimination between
470 potential sources is clearly shown by the LDA biplot analysis. However, in none of the
471 combinations tested, there was a clear distinction between potential source groups.
472 According to the distribution of dots and ellipses, there is an overlap of groups,
473 especially for the approaches UV and MUV. The combination of GEO with the other sets
474 of tracers, M and UV, improved the discrimination between two groups: surface
475 (pasture and cropland) and subsurface sources (stream bank, unpaved road and gully).
476 The lack of clear discrimination evident in the LDA biplots likely adds uncertainty to the
477 model results.

478 The soils of the catchment are naturally poor in K and P, two of the main
479 macronutrients essential for crop growth and productivity. The addition of fertilizers in
480 croplands and pastures explains the higher concentration of these elements in surface
481 sources, which differed significantly from those found in subsurface sources. The TOC
482 concentration in the Ferralsols of the region is usually higher in the upper layer of the
483 soil, due to the addition of carbon by the plant residues and roots, as observed in a study
484 of Bortolon et al. (2011), where soil analyses had a mean concentration 1.5 times higher
485 in the uppermost 10 cm of the soil compared to the 10-20 cm layer. Indeed, these three
486 tracers (P, K and TOC) have great potential for tracing agricultural land uses. However,
487 the three geochemical tracers selected in the current research (P, TOC and K) are

488 usually removed from analysis in most sediment fingerprinting studies, as they are
489 generally considered to be easily enriched or depleted during the erosion process
490 (Palazón and Navas, 2017b; Smith and Blake, 2014). Even though, most studies end up
491 discarding these elements without performing any range tests to assess their
492 conservativeness. For example, in an evaluation of 60 studies that evaluated P as a
493 potential tracer, only 27 of them applied a range test, and of these, P was conservative in
494 85% of cases (Tiecher et al., 2019). Moreover, this parameter was selected to model
495 source contributions in 43% of the 60 sediment fingerprinting studies that were
496 reviewed in Tiecher et al. (2019).

497 The transformation of the sediment composition during the erosion and river
498 transport processes is variable depending on the study site considered. The TOC levels
499 found in sediment samples collected in a previous study conducted in the Conceição
500 River catchment (Tiecher et al., 2018) had a lower concentration in the target material
501 compared to that found in the sources, while in the study of Pulley et al. (2015a)
502 sediment was found to be enriched in TOC compared to potential sources. In
503 catchments with strongly weathered soils rich in iron oxides, P is known to be mainly
504 transported in particulate form in the rivers (Bender et al., 2018). This strong chemical
505 adsorption to soil and sediment particles may preserve the P source signature during
506 their transfer in river systems. The no-tillage farming that is main soil management
507 system in the Conceição catchment in soils with a high content of clay and iron oxides
508 may have induced the physico-chemical protection of C and P into micro aggregates (Six
509 et al., 2002; Snyder and Vázquez, 2005). TOC and P are highly correlated as shown in
510 Figure 3, and the strong physical-chemical protection of these elements may support
511 their conservative behaviour. Furthermore, the conservative behaviour of Fe
512 demonstrates that the reduction from its solid state (oxides with Fe³⁺) to the aqueous

513 one (Fe^{2+}) is not an important process during sediment transport in this catchment,
514 allowing the conservation of the source characteristics.

515 Soil organic carbon, water content, iron oxides and chemical composition are the
516 main parameters responsible for the soil colour (Ben-dor et al., 1998). Although the TOC
517 content had a low correlation with the colour parameters, this parameter can create a
518 source of error in the colour indices, especially when there is a small colour difference
519 between the potential sources (Pulley and Rowntree, 2016a). The soils of the Conceição
520 River catchment are rich in iron oxides, mainly found as goethite and hematite, and
521 colour parameters are closely linked to their respective content in the soils (Schaefer et
522 al., 2008). The A3 index, which is related to the electron pair transition of hematite, have
523 a strong correlation with most colour parameters (data not presented), highlighting the
524 importance of iron oxides in defining the soils and sediment colours in this catchment.
525 Hematite is responsible for the red colour of Ferralsols, while goethite is responsible for
526 the brownish-reddish yellow colour of soils (Cornell and Schwertmann, 2003). The Hr
527 index, which cannot be used in the mixing model because it is not linearly additive,
528 represents the proportion of hematite in the pool of iron oxides (goethite + hematite).
529 Although the soils in the region are predominantly red in colour, their content in
530 goethite is higher than in hematite (Ramos et al., 2020). The Hr index had lower values
531 in the stream banks compared to the other sources, since there is a greater tendency to
532 form goethite in relief positions characterised by the accumulation of water, where
533 ferrihydrite tends to dissolve and form goethite in its place (Schaefer et al., 2008).

534 Owing to the homogeneity of the soil types due to their intense chemical
535 weathering found in the Conceição catchment, the difference in colour and iron oxide
536 parameters between land uses (pastures and croplands) is very low. Differences
537 between surface and subsurface sources tend to be more evident, since a difference in

538 TOC and clay content is usually observed in this type of soils (Table 4) (Testoni et al.,
539 2017). A similar observation is valid for magnetic parameters, which are closely related
540 to the ferromagnetic properties of the soil, which are in turn mainly controlled by
541 particle size and the nature of parent material (Pulley and Rowntree, 2016b). As the
542 potential sources evaluated are originated from very similar soil types and parent
543 material in our catchment, M and UV parameters did not improve significantly the
544 discrimination between land use-based sources.

545 In the same way as with the GEO parameters selected, UV and M likely provided
546 stronger discrimination between surface and subsurface sources. When UV parameters
547 were used in isolation, they were able to classify correctly almost 60% of the samples in
548 their respective groups, which is not so different from the %SCC obtained with GEO
549 tracers alone (68%), according to the LDA. This demonstrates the potential of UV and M
550 tracers to provide a low-cost alternative to GEO tracers. Although UV parameters were
551 not very effective alone in the current research, they have already been used
552 successfully in other case studies (Evrard et al., 2019; Pulley et al., 2018).

553 The low conservativeness of the tracers tested may also be associated with
554 particle size issues (Lacey et al., 2017). Owing to time and financial constraints it was
555 not possible to conduct particle size analyses. Future studies should also consider
556 assessing how particle size may affect conservativeness during erosion, transport and
557 deposition processes in large river catchments. Furthermore, clay soils with high levels
558 of iron oxides, as observed in the present catchment, often form strong stable
559 microaggregates, during erosion process and transport processes, which may behave
560 similarly to coarse particles (silt and sand) (Droppo et al, 2005). Future research should
561 therefore investigate how microaggregates may also affect tracer conservativeness in
562 sediment fingerprinting research in large scale catchments.

563 4.2 Mixing model results

564 The results of the mixing model are impacted by the relatively bad quality of the
565 sediment source discrimination. The small difference in tracer signature observed
566 within a given group (surface or subsurface) introduces high uncertainties in the mixing
567 model (Pulley et al., 2017a). The mixing model results in a large IQR, which means that
568 the uncertainty in the model predictions is high. However, the mean results are similar
569 to those observed by Tiecher et al. (2018), who showed that surface sources provided
570 the main source of suspended sediment collected following the TISS strategy, and
571 subsurface sources, mainly stream bank, supplied the main source for FBS samples. The
572 model results according to the different sets of tracers were consistent and there were
573 no major differences between them. Although there is some correlation between the
574 selected parameters in each approach (Figure 3), the potential effect of this collinearity
575 cannot be tested without artificial mixtures, which should be recommended for future
576 research.

577 Pasture and cropland were poorly distinguished by the discriminant analysis. As
578 a consequence, the mixing model predicted a larger contribution of pastures, which is
579 not consistent with the situation observed in the catchment, where the percentage of
580 land use occupied by pasture is much lower (maximum of 11.9%) and where soil
581 erosion remains limited under this land use. Unpaved roads provided the source that
582 contributed the least to sediment, as observed by Tiecher et al. (2018). Considering the
583 mean source contributions obtained in the current research, they remained consistent
584 with our overall understanding of the hydro-sedimentary behaviour of the catchment,
585 although the high uncertainties associated with the model predictions limited the
586 potential use that could be made of these calculated contributions (e.g. for catchment
587 and river management). In that, the results of the current research strongly differed

588 from those of Chen et al. (2019), who obtained a good discrimination between land uses
589 using the geochemical composition in a catchment with similar geological conditions in
590 the Three Gorges Dam Region, China. However, this study was conducted in two small
591 catchments (0.78 and 0.46 km²) with shallow (< 50 cm depth) and poorly developed
592 soils with rock fragments, and land use management was also very different.
593 Accordingly, this shows that considering the homogeneity of geological conditions is not
594 sufficient to derive the tracer list as different pedogenic processes and land use
595 management may impact the tracing properties.

596 The selection of tracers to be used in each study is generally defined by the
597 constraints of financial resources and access to the analytical facilities (Collins et al.,
598 2017a). However, the priority should be given to the physico-chemical basis supporting
599 the potential sediment source. UV or M properties are often suggested as low cost
600 tracers, but in a catchment with limited geological variability and intense chemical
601 weathering such as under tropical conditions, their use is not straightforward. Indeed,
602 soils had almost homogeneous chemical compositions and a reddish colour through the
603 whole soil profile. Under these conditions, UV had low variability and does not provide a
604 good tracer for discriminating land use-based sources. The need to add a set of different
605 tracers in sediment fingerprinting studies is expected to increase as geological and soil
606 type variability increases in the catchment, as well as the number of sources of interest
607 increases.

608 As a consequence, the discrimination between the sources achieved in the
609 current research remained low, and the modelling results uncertain. Furthermore, as
610 observed by Haddadchi et al. (2013), mixing models may lead to different results
611 depending on the input data. To avoid this problem, the use of tracers with >90% of SCC
612 or the preparation of artificial mixtures for model validation should be systematically

613 recommended in future sediment fingerprinting approaches. Indeed, there may simply
614 be limitations to the efficacy of the sediment fingerprinting technique in catchments
615 with homogeneous geology or soil types that can be found in many regions of the world,
616 mainly under tropical climates where soils are highly weathered.

617 A significant proportion of the most productive soils around the world are found
618 under these conditions, and this situation strengthens the need to develop new
619 approaches to discriminate between these land use-based sources. Alternative tracers
620 such as environmental DNA (Foucher et al., 2020) and compound specific stable
621 isotopes (CSSI) (Blake et al., 2012) may provide a powerful alternative to trace the
622 contribution of specific land use sources to sediment. However, technical solutions
623 allowing for the global application of these methods still need to be developed (Brandt
624 et al., 2018; Evrard et al., 2019). Moreover, the application of these vegetation specific
625 related tracers maybe even more challenging in large tropical catchments, characterised
626 by transient and heterogeneous land uses which are often scarcely documented.
627 Accordingly, their use in combination with more conventional tracers may provide a
628 solution to provide consistent and reliable estimations of sediment source contributions
629 to help achieving sustainable agricultural development goals in these regions.

630 **5 Conclusions**

631 The use of alternative tracers based on ultraviolet-visible spectra combined with
632 geochemical parameters improved the sediment source discrimination in the Conceição
633 River catchment. However, the low differences in source signatures observed in this
634 study site resulted in high uncertainties associated with the model predictions, which is
635 mainly due to the homogeneous soil types occurring in the catchment, which are highly
636 weathered and which have a low variability between land uses, as well as between

637 surface and subsurface sources. Furthermore, in such a homogeneous catchment, the
638 low differences between sources observed for almost all the tested parameters
639 increased the probability of sediments to lie outside of the range observed in the
640 sources and to be removed by the range/conservative tests, which further reduced the
641 number of tracer options.

642 Magnetic, geochemical and ultraviolet-visible derived parameters have proven to
643 be relatively ineffective for tracing land use-based sources in the Conceição River
644 catchment. When using only one set of tracers, which does not provide a robust
645 discrimination between the sources leading to low percentages of correctly classified
646 samples by the LDA, the results of the model should be used with caution, since they are
647 associated with large uncertainties. This study presents results that differ from those
648 commonly observed in the literature, where additional tracers generally have positive
649 results, showing that the sediment fingerprinting technique may not provide
650 meaningful results in all situations. Tracers with a greater potential for land use
651 discrimination, such as environmental DNA or CSSI, could provide an alternative for
652 better understanding soil erosion processes in the Conceição River catchment and other
653 similar homogeneous catchments worldwide. As such, future research should
654 investigate the efficacy of these next generation tracers in increasingly difficult tracing
655 environments with more attention to the potential impact of particle size on them.

656

657 **6 Acknowledgments**

658 The authors would like to thank to Conselho Nacional de Pesquisa - CNPq,
659 Coordenação de Aperfeiçoamento de Pessoal de Nível Superior - CAPES, Financiadora
660 de Estudos e Projetos – FINEP for providing financial support. Furthermore, the authors

661 are grateful to the “Mais Água” and FAPERGS PRONEX n° 008/2009 projects for their
662 support. The authors are also grateful to CAPES for founding the PhD scholarship of the
663 first author Rafael Ramon in the framework of the CAPES-COFECUB Project No.
664 88887.196234/2018-00.

665

666 **7 References**

667 Almagro, Andre, Almagro, André, Oliveira, P.T.S., Nearing, M.A., Hagemann, S., 2017.
668 Projected climate change impacts in rainfall erosivity over Brazil Projected climate
669 change impacts in rainfall erosivity over Brazil 0–12.
670 <https://doi.org/10.1038/s41598-017-08298-y>

671 Anache, J.A.A., Wendland, E.C., Oliveira, P.T.S., Flanagan, D.C., Nearing, M.A., 2017. Runoff
672 and soil erosion plot-scale studies under natural rainfall: A meta-analysis of the
673 Brazilian experience. CATENA 152, 29–39.
674 <https://doi.org/10.1016/j.catena.2017.01.003>

675 Batista, P.V.G., Laceby, J.P., Silva, M.L.N., Tassinari, D., Bispo, D.F.A., Curi, N., Davies, J.,
676 Quinton, J.N., 2018. Using pedological knowledge to improve sediment source
677 apportionment in tropical environments. J. Soils Sediments.
678 <https://doi.org/10.1007/s11368-018-2199-5>

679 Belmont, P., Willenbring, J.K., Schottler, S.P., Marquard, J., Kumarasamy, K., Hemmis, J.M.,
680 2014. Toward generalizable sediment fingerprinting with tracers that are
681 conservative and nonconservative over sediment routing timescales. J. Soils
682 Sediments 14, 1479–1492. <https://doi.org/10.1007/s11368-014-0913-5>

683 Ben-dor, E., Irons, J., Epema, G.F., 1998. Soil Reflectance, in: Rencz, A.N. (Ed.), Remote
684 Sensing for the Earth Sciences. Manual of Remote Sensing. John Wiley & Sons, Ltd,

685 New York, pp. 111–188.

686 Bender, M.A., dos Santos, D.R., Tiecher, T., Minella, J.P.G., de Barros, C.A.P., Ramon, R.,
687 2018. Phosphorus dynamics during storm events in a subtropical rural catchment
688 in southern Brazil. *Agric. Ecosyst. Environ.* 261.
689 <https://doi.org/10.1016/j.agee.2018.04.004>

690 Blake, W.H., Ficken, K.J., Taylor, P., Russell, M.A., Walling, D.E., 2012. Tracing crop-
691 specific sediment sources in agricultural catchments. *Geomorphology* 139–140,
692 322–329. <https://doi.org/10.1016/j.geomorph.2011.10.036>

693 Boardman, J., Vandaele, K., Evans, R., Foster, I.D.L., 2019. Off-site impacts of soil erosion and
694 runoff: Why connectivity is more important than erosion rates. *Soil Use Manag.* 35,
695 245–256. <https://doi.org/10.1111/sum.12496>

696 Bortolon, E.S.O., Mielniczuk, J., Tornquist, C.G., Lopes, F., Bergamaschi, H., 2011.
697 Validation of the Century model to estimate the impact of agriculture on soil
698 organic carbon in Southern Brazil. *Geoderma* 167–168, 156–166.
699 <https://doi.org/10.1016/j.geoderma.2011.08.008>

700 Borrelli, P., Robinson, D.A., Fleischer, L.R., Lugato, E., Ballabio, C., Alewell, C.,
701 Meusburger, K., Modugno, S., Schütt, B., Ferro, V., Bagarello, V., Oost, K. Van,
702 Montanarella, L., Panagos, P., 2017. An assessment of the global impact of 21st
703 century land use change on soil erosion. *Nat. Commun.* 8, 2013.
704 <https://doi.org/10.1038/s41467-017-02142-7>

705 Brandt, C., Dercon, G., Cadisch, G., Nguyen, L.T., Schuller, P., Linares, C.B., Santana, A.C.,
706 Golosov, V., Benmansour, M., Amenzou, N., Xinbao, Z., Rasche, F., 2018. Towards
707 global applicability? Erosion source discrimination across catchments using
708 compound-specific $\delta^{13}\text{C}$ isotopes. *Agric. Ecosyst. Environ.* 256, 114–122.
709 <https://doi.org/10.1016/j.agee.2018.01.010>

710 Brosinsky, A., Foerster, S., Segl, K., Kaufmann, H., 2014a. Spectral fingerprinting:

711 sediment source discrimination and contribution modelling of artificial mixtures
712 based on VNIR-SWIR spectral properties. *J. Soils Sediments* 14, 1949–1964.
713 <https://doi.org/10.1007/s11368-014-0925-1>

714 Brosinsky, A., Foerster, S., Segl, K., López-Tarazón, J.A., Piqué, G., Bronstert, A., 2014b.
715 Spectral fingerprinting: characterizing suspended sediment sources by the use of
716 VNIR-SWIR spectral information. *J. Soils Sediments* 14, 1965–1981.
717 <https://doi.org/10.1007/s11368-014-0927-z>

718 Caner, L., Petit, S., Joussein, E., Fritsch, E., Herbillon, A.J., 2011. Accumulation of organo-
719 metallic complexes in laterites and the formation of Aluandic Andosols in the
720 Nilgiri Hills (southern India): similarities and differences with Umbric Podzols. *Eur.*
721 *J. Soil Sci.* 62, 754–764. <https://doi.org/10.1111/j.1365-2389.2011.01389.x>

722 Chen, F., Wang, X., Li, X., Wang, J., Xie, D., Ni, J., Liu, Y., 2019. Using the sediment
723 fingerprinting method to identify the sediment sources in small catchments with
724 similar geological conditions. *Agric. Ecosyst. Environ.* 286, 106655.
725 <https://doi.org/10.1016/j.agee.2019.106655>

726 Chen, M., Ma, L.Q., 2001. Comparison of Three Aqua Regia Digestion Methods for Twenty
727 Florida Soils. *Soil Sci. Soc. Am. J.* 65, 491–499.
728 <https://doi.org/10.2136/sssaj2001.652491x>

729 CIE, 1978. Commission Internationale d’Eclairage. Recommendations on Uniform
730 Colour Spaces, Colour Difference Equations, Psychometric Colour Terms. *J. Oral*
731 *Rehabil.*

732 CIE, C.I. de l’Eclairage, 1931. Commission Internationale de l’Eclairage (CIE), in: CIE
733 Proceedings. Cambridge University Press, Cambridge, UK.

734 Collins, A.L., Foster, I.D.L., Gellis, A.C., Porto, P., Horowitz, A.J., 2017a. Sediment source
735 fingerprinting for informing catchment management: Methodological approaches,

736 problems and uncertainty. *J. Environ. Manage.* 194, 1–3.
737 <https://doi.org/10.1016/j.jenvman.2017.03.026>

738 Collins, A.L., Pulley, S., Foster, I.D.L., Gellis, A., Porto, P., Horowitz, A.J., 2017b. Sediment
739 source fingerprinting as an aid to catchment management: A review of the current
740 state of knowledge and a methodological decision-tree for end-users. *J. Environ.*
741 *Manage.* 194, 86–108. <https://doi.org/10.1016/j.jenvman.2016.09.075>

742 Collins, A.L., Walling, D.E., Webb, L., King, P., 2010a. Apportioning catchment scale
743 sediment sources using a modified composite fingerprinting technique
744 incorporating property weightings and prior information. *Geoderma* 155, 249–261.
745 <https://doi.org/10.1016/j.geoderma.2009.12.008>

746 Collins, A.L., Zhang, Y., Walling, D.E., 2010b. Apportioning sediment sources in a
747 grassland dominated agricultural catchment in the UK using a new tracing
748 framework. *Sediment Dyn. a Chang. Futur.* 337, 68–75.

749 Cornell, R.M., Schwertmann, U., 2003. The iron oxides. Structure, properties, reactions,
750 occurrences and uses, Second. ed. WILEY-VCH Verlag GmbH & Co. KGaA, Weinheim.

751 Da Silva, Y.J.A.B., Do Nascimento, C.W.A., Biondi, C.M., 2014. Comparison of USEPA
752 digestion methods to heavy metals in soil samples. *Environ. Monit. Assess.* 186, 47–
753 53. <https://doi.org/10.1007/s10661-013-3354-5>

754 Didoné, E.J., Gomes Minella, J.P., Andres Schneider, F.J., Londero, A.L., Lefèvre, I., Evrard,
755 O., 2019. Quantifying the impact of no-tillage on soil redistribution in a cultivated
756 catchment of Southern Brazil (1964–2016) with ¹³⁷Cs inventory measurements.
757 *Agric. Ecosyst. Environ.* 284, 106588. <https://doi.org/10.1016/j.agee.2019.106588>

758 Didoné, E.J., Minella, J.P.G., Merten, G.H., 2015. Quantifying soil erosion and sediment
759 yield in a catchment in southern Brazil and implications for land conservation. *J.*
760 *Soils Sediments* 15, 2334–2346. <https://doi.org/10.1007/s11368-015-1160-0>

761 Droppo, I.G., Nackaerts, K., Walling, D.E., Williams, N., 2005. Can flocs and water stable

762 soil aggregates be differentiated within fluvial systems? CATENA 60, 1–18.
763 <https://doi.org/10.1016/j.catena.2004.11.002>

764 EPA, U.S., 2007. “Method 3051A (SW-846): Microwave Assisted Acid Digestion of
765 Sediments, Sludges, and Oils,” Revision 1. Washington, D.C.

766 Evrard, O., Durand, R., Foucher, A., Tiecher, T., Sellier, V., Onda, Y., Lefèvre, I., Cerdan, O.,
767 Laceby, J.P., 2019. Using spectrocolourimetry to trace sediment source dynamics in
768 coastal catchments draining the main Fukushima radioactive pollution plume
769 (2011–2017). *J. Soils Sediments*. <https://doi.org/10.1007/s11368-019-02302-w>

770 Evrard, O., Laceby, J.P., Ficetola, G.F., Gielly, L., Huon, S., Lefèvre, I., Onda, Y., Poulénard, J.,
771 2019. Environmental DNA provides information on sediment sources: A study in
772 catchments affected by Fukushima radioactive fallout. *Sci. Total Environ.* 665, 873–
773 881. <https://doi.org/10.1016/j.scitotenv.2019.02.191>

774 FAO, 2019. Soil erosion: the greatest challenge for sustainable soil management. Licence:
775 CC BY-NC-SA 3.0 IGO, Rome.

776 Foucher, A., Evrard, O., Ficetola, G.F., Gielly, L., Poulain, J., Giguët-Covex, C., Laceby, J.P.,
777 Salvador-Blanes, S., Cerdan, O., Poulénard, J., 2020. Persistence of environmental
778 DNA in cultivated soils: implication of this memory effect for reconstructing the
779 dynamics of land use and cover changes. *Sci. Rep.* 10, 1–12.
780 <https://doi.org/10.1038/s41598-020-67452-1>

781

782 Fritsch, E., Morin, G., Bedidi, A., Bonnin, D., Balan, E., Caquineau, S., Calas, G., 2005.
783 Transformation of haematite and Al-poor goethite to Al-rich goethite and
784 associated yellowing in a ferralitic clay soil profile of the middle Amazon Basin
785 (Manaus, Brazil). *Eur. J. Soil Sci.* 56, 575–588. [https://doi.org/10.1111/j.1365-](https://doi.org/10.1111/j.1365-2389.2005.00693.x)
786 [2389.2005.00693.x](https://doi.org/10.1111/j.1365-2389.2005.00693.x)

787 Gaspar, L., Blake, W.H., Smith, H.G., Lizaga, I., Navas, A., 2019. Testing the sensitivity of a

788 multivariate mixing model using geochemical fingerprints with artificial mixtures.
789 *Geoderma* 337, 498–510. <https://doi.org/10.1016/j.geoderma.2018.10.005>

790 Guzmán, G., Quinton, J.N., Nearing, M.A., Mabit, L., Gómez, J.A., 2013. Sediment tracers in
791 water erosion studies: Current approaches and challenges. *J. Soils Sediments* 13,
792 816–833. <https://doi.org/10.1007/s11368-013-0659-5>

793 Haddadchi, A., Ryder, D.S., Evrard, O., OLLEY, J., 2013. Sediment fingerprinting in fluvial
794 systems: review of tracers, sediment sources and mixing models. *Int. J. Sediment*
795 *Res.* 28, 560–578. [https://doi.org/10.1016/S1001-6279\(14\)60013-5](https://doi.org/10.1016/S1001-6279(14)60013-5)

796 Hatfield, J.L., Sauer, T.J., Cruse, R.M., 2017. *Soil : The Forgotten Piece of the Water , Food ,*
797 *Energy Nexus*, 1st ed, *Advances in Agronomy*. Elsevier Inc.
798 <https://doi.org/10.1016/bs.agron.2017.02.001>

799 HunterLab, 2015. The basics of color perception and measurement [WWW Document].
800 URL <https://www.hunterlab.com/basics-of-color-theory.pdf?r=false> (accessed
801 7.9.19).

802 Jia, L., Zhao, W., Zhai, R., Liu, Y., Kang, M., Zhang, X., 2019. Regional differences in the soil
803 and water conservation efficiency of conservation tillage in China. *Catena* 175, 18–
804 26. <https://doi.org/10.1016/j.catena.2018.12.012>

805 Koiter, A.J., Owens, P.N., Petticrew, E.L., Lobb, D.A., 2013. The behavioural characteristics
806 of sediment properties and their implications for sediment fingerprinting as an
807 approach for identifying sediment sources in river basins. *Earth-Science Rev.* 125,
808 24–42. <https://doi.org/10.1016/j.earscirev.2013.05.009>

809 Kosmas, C.S., Curi, N., Bryant, R.B., Franzmeier, D.P., 1984. Characterization of iron oxide
810 minerals by second-derivative visible spectroscopy. *Soil Sci. Soc. Am. J.* 48, 401–
811 405. <https://doi.org/10.2136/sssaj1984.03615995004800020036x>

812 Laceby, J.P., Evrard, O., Smith, H.G., Blake, W.H., Olley, J.M., Minella, J.P.G., Owens, P.N.,

813 2017. The challenges and opportunities of addressing particle size effects in
814 sediment source fingerprinting: A review. *Earth-Science Rev.* 169, 85–103.
815 <https://doi.org/10.1016/j.earscirev.2017.04.009>

816 Lal, R., 2007. Anthropogenic Influences on World Soils and Implications to Global Food
817 Security. *Adv. Agron.* 93, 69–93. [https://doi.org/10.1016/S0065-2113\(06\)93002-8](https://doi.org/10.1016/S0065-2113(06)93002-8)

818 Legout, C., Poulenard, J., Nemery, J., Navratil, O., Grangeon, T., Evrard, O., Esteves, M.,
819 2013. Quantifying suspended sediment sources during runoff events in headwater
820 catchments using spectrophotometry. *J. Soils Sediments* 13, 1478–1492.
821 <https://doi.org/10.1007/s11368-013-0728-9>

822 Lizaga, I., Latorre, B., Gaspar, L., Navas, A., 2020. Consensus ranking as a method to
823 identify non-conservative and dissenting tracers in fingerprinting studies. *Sci. Total*
824 *Environ.* 720, 137537. <https://doi.org/10.1016/j.scitotenv.2020.137537>

825 López-Mársico, L., Altesor, A., Oyarzabal, M., Baldassini, P., Paruelo, J.M., 2015. Grazing
826 increases below-ground biomass and net primary production in a temperate
827 grassland. *Plant Soil* 392, 155–162. <https://doi.org/10.1007/s11104-015-2452-2>

828 Martínez-Carreras, N., Krein, A., Gallart, F., Iffly, J.F., Pfister, L., Hoffmann, L., Owens, P.N.,
829 2010a. Assessment of different colour parameters for discriminating potential
830 suspended sediment sources and provenance: A multi-scale study in Luxembourg.
831 *Geomorphology* 118, 118–129. <https://doi.org/10.1016/j.geomorph.2009.12.013>

832 Martínez-Carreras, N., Udelhoven, T., Krein, A., Gallart, F., Iffly, J.F., Ziebel, J., Hoffmann,
833 L., Pfister, L., Walling, D.E., 2010b. The use of sediment colour measured by diffuse
834 reflectance spectrometry to determine sediment sources: Application to the Attert
835 River catchment (Luxembourg). *J. Hydrol.* 382, 49–63.
836 <https://doi.org/10.1016/j.jhydrol.2009.12.017>

837 Melo, D.C.D., Anache, J.A.A., Almeida, C. das N., Coutinho, J. V., Ramos Filho, G.M.,
838 Rosalem, L.M.P., Pelinson, N.S., Ferreira, G.L.R.A., Schwaback, D., Calixto, K.G.,

839 Siqueira, J.P.G., Duarte-Carvajalino, J.C., Jhuniór, H.C.S., Nóbrega, J.D., Morita, A.K.M.,
840 Leite, C.M.C., Guedes, A.C.E., Coelho, V.H.R., Wendland, E., 2020. The big picture of
841 field hydrology studies in Brazil. *Hydrol. Sci. J.* 0, 1.
842 <https://doi.org/10.1080/02626667.2020.1747618>

843 Minella, J.P.G., Merten, G.H., Clarke, R.T., 2004. Identification of sediment sources in a
844 small rural drainage basin, in: *Sediment Transfer through the Fluvial System*
845 (Proceedings of a Symposium Held in Moscow, August 2004). IAHS Press, Moscow,
846 pp. 44–51.

847 Mullins, C.E., 1977. Magnetic Susceptibility of the Soil and Its Significance in Soil Science
848 – a Review. *J. Soil Sci.* 28, 223–246. [https://doi.org/10.1111/j.1365-](https://doi.org/10.1111/j.1365-2389.1977.tb02232.x)
849 [2389.1977.tb02232.x](https://doi.org/10.1111/j.1365-2389.1977.tb02232.x)

850 Navratil, O., Evrard, O., Esteves, M., Legout, C., Ayrault, S., Némery, J., Mate-Marin, A.,
851 Ahmadi, M., Lefèvre, I., Poirel, A., Bonté, P., 2012. Temporal variability of suspended
852 sediment sources in an alpine catchment combining river/rainfall monitoring and
853 sediment fingerprinting. *Earth Surf. Process. Landforms* 37, 828–846.
854 <https://doi.org/10.1002/esp.3201>

855 Niu, B., Zhang, X., Qu, J., Liu, B., Homan, J., Tan, L., An, Z., 2019. Using multiple composite
856 fingerprints to quantify source contributions and uncertainties in an arid region. *J.*
857 *Soils Sediments*. <https://doi.org/10.1007/s11368-019-02424-1>

858 Nosrati, K., Collins, A.L., 2019. Investigating the importance of recreational roads as a
859 sediment source in a mountainous catchment using a fingerprinting procedure
860 with different multivariate statistical techniques and a Bayesian un-mixing model.
861 *J. Hydrol.* 569, 506–518. <https://doi.org/10.1016/j.jhydrol.2018.12.019>

862 Palazón, L., Navas, A., 2017a. Variability in source sediment contributions by applying
863 different statistic test for a Pyrenean catchment. *J. Environ. Manage.* 194, 42–53.
864 <https://doi.org/10.1016/j.jenvman.2016.07.058>

865 Palazón, L., Navas, A., 2017b. Variability in source sediment contributions by applying

866 different statistic test for a Pyrenean catchment. *J. Environ. Manage.* 194, 42–53.
867 <https://doi.org/10.1016/j.jenvman.2016.07.058>

868 Phillips, J.M., Russell, M.A., Walling, D.E., 2000. Time-integrated sampling of fluvial
869 suspended sediment: A simple methodology for small catchments. *Hydrol. Process.*
870 14, 2589–2602. [https://doi.org/10.1002/1099-1085\(20001015\)14:14<2589::AID-](https://doi.org/10.1002/1099-1085(20001015)14:14<2589::AID-HYP94>3.0.CO;2-D)
871 [HYP94>3.0.CO;2-D](https://doi.org/10.1002/1099-1085(20001015)14:14<2589::AID-HYP94>3.0.CO;2-D)

872 Pimentel, D., 2006. Soil Erosion: A Food and Environmental Threat. *Environ. Dev.*
873 *Sustain.* 8, 119–137. <https://doi.org/10.1007/s10668-005-1262-8>

874 Poesen, J., 2017. Soil erosion in the Anthropocene: research needs. *Earth Surf. Process.*
875 *Landforms* 84, 64–84. <https://doi.org/10.1002/esp.4250>

876 Poulencard, J., Legout, C., Némery, J., Bramorski, J., Navratil, O., Douchin, A., Fanget, B.,
877 Perrette, Y., Evrard, O., Esteves, M., 2012. Tracing sediment sources during floods
878 using Diffuse Reflectance Infrared Fourier Transform Spectrometry (DRIFTS): A
879 case study in a highly erosive mountainous catchment (Southern French Alps). *J.*
880 *Hydrol.* 414–415, 452–462. <https://doi.org/10.1016/j.jhydrol.2011.11.022>

881 Pulley, S., Foster, I., Antunes, P., 2015a. The uncertainties associated with sediment
882 fingerprinting suspended and recently deposited fluvial sediment in the Nene river
883 basin. *Geomorphology* 228, 303–319.
884 <https://doi.org/10.1016/j.geomorph.2014.09.016>

885 Pulley, S., Foster, I., Antunes, P., 2015b. The application of sediment fingerprinting to
886 floodplain and lake sediment cores: assumptions and uncertainties evaluated
887 through case studies in the Nene Basin, UK. *J. Soils Sediments* 15, 2132–2154.
888 <https://doi.org/10.1007/s11368-015-1136-0>

889 Pulley, S., Foster, I., Collins, A.L., 2017a. The impact of catchment source group
890 classification on the accuracy of sediment fingerprinting outputs. *J. Environ.*

891 Manage. 194, 16–26. <https://doi.org/10.1016/j.jenvman.2016.04.048>

892 Pulley, S., Rowntree, K., 2016a. The use of an ordinary colour scanner to fingerprint
893 sediment sources in the South African Karoo. *J. Environ. Manage.* 165, 253–262.
894 <https://doi.org/10.1016/j.jenvman.2015.09.037>

895 Pulley, S., Rowntree, K., 2016b. Stages in the life of a magnetic grain: Sediment source
896 discrimination, particle size effects and spatial variability in the South African
897 Karoo. *Geoderma* 271, 134–143. <https://doi.org/10.1016/j.geoderma.2016.02.015>

898 Pulley, S., Van Der Waal, B., Collins, A.L., Foster, I.D.L., Rowntree, K., 2017b. Are source
899 groups always appropriate when sediment fingerprinting? The direct comparison
900 of source and sediment samples as a methodological step. *River Res. Appl.* 33,
901 1553–1563. <https://doi.org/10.1002/rra.3192>

902 Pulley, S., Van der Waal, B., Rowntree, K., Collins, A.L., 2018. Colour as reliable tracer to
903 identify the sources of historically deposited flood bench sediment in the Transkei,
904 South Africa: A comparison with mineral magnetic tracers before and after
905 hydrogen peroxide pre-treatment. *CATENA* 160, 242–251.
906 <https://doi.org/10.1016/j.catena.2017.09.018>

907 R Development Core Team, 2017. R: a language and environment for statistical
908 computing.

909 Ramon, R., Minella, J.P.G., Merten, G.H., de Barros, C.A.P., Canale, T., 2017. Kinetic energy
910 estimation by rainfall intensity and its usefulness in predicting
911 hydrosedimentological variables in a small rural catchment in southern Brazil.
912 *CATENA* 148, 176–184. <https://doi.org/10.1016/j.catena.2016.07.015>

913 Ramos, P.V., Indaa, A.V., Barrón, V., Siqueira, D.S., Júnior, J., Teixeira, D.D.B., 2020. Color
914 in subtropical brazilian soils as determined with a Munsell chart and by diffuse
915 reflectance spectroscopy. *Catena* 193, 1–26.
916 <https://doi.org/10.1016/j.catena.2020.104609>

917 Rencher, A.C., 2005. A Review Of "Methods of Multivariate Analysis, Second Edition." IIE
918 Trans. 37, 1083–1085. <https://doi.org/10.1080/07408170500232784>

919 Rowntree, K.M., van der Waal, B.W., Pulley, S., 2017. Magnetic susceptibility as a simple
920 tracer for fluvial sediment source ascription during storm events. J. Environ.
921 Manage. 194, 54–62. <https://doi.org/10.1016/j.jenvman.2016.11.022>

922 Schaefer, C.E.G.R., Fabris, J.D., Ker, J.C., 2008. Minerals in the clay fraction of Brazilian
923 Latosols (Oxisols): a review. Clay Miner. 43, 137–154.
924 <https://doi.org/10.1180/claymin.qw2008.043.1.11>

925 Scheinost, A.C., Chavernas, A., Barrón, V., Torrent, J., 1998. Use and limitations of second-
926 derivative diffuse reflectance spectroscopy in the visible to near-infrared range to
927 identify and quantify Fe oxide minerals in soils. Clays Clay Miner. 46, 528–536.
928 <https://doi.org/10.1346/CCMN.1998.0460506>

929 Schuman, G.E., Reeder, J.D., Manley, J.T., Hart, R.H., Manley, W.A., 1999. Impact of grazing
930 management on the carbon and nitrogen balance of a mixed-grass rangeland. Ecol.
931 Appl. 9, 65–71. [https://doi.org/10.1890/1051-0761\(1999\)009\[0065:IOGMOT\]2.0.CO;2](https://doi.org/10.1890/1051-0761(1999)009[0065:IOGMOT]2.0.CO;2)

932

933 Sherriff, S.C., Franks, S.W., Rowan, J.S., Fenton, O., Ó'hUallacháin, D., 2015. Uncertainty-
934 based assessment of tracer selection, tracer non-conservativeness and multiple
935 solutions in sediment fingerprinting using synthetic and field data. J. Soils
936 Sediments 15, 2101–2116. <https://doi.org/10.1007/s11368-015-1123-5>

937 Six, J., Feller, C., Denef, K., Ogle, S.M., de Moraes, J.C., Albrecht, A., 2002. Soil organic
938 matter, biota and aggregation in temperate and tropical soils - Effects of no-tillage.
939 Agronomie 22, 755–775. <https://doi.org/10.1051/agro:2002043>

940 Smith, H.G., Blake, W.H., 2014. Sediment fingerprinting in agricultural catchments: A
941 critical re-examination of source discrimination and data corrections.

942 Geomorphology 204, 177–191. <https://doi.org/10.1016/j.geomorph.2013.08.003>

943 Smith, H.G., Evrard, O., Blake, W.H., Owens, P.N., 2015. Preface—Addressing challenges
944 to advance sediment fingerprinting research. *J. Soils Sediments* 15, 2033–2037.
945 <https://doi.org/10.1007/s11368-015-1231-2>

946 Smith, H.G., Karam, D.S., Lennard, A.T., 2018. Evaluating tracer selection for catchment
947 sediment fingerprinting. *J. Soils Sediments* 18, 3005–3019.
948 <https://doi.org/10.1007/s11368-018-1990-7>

949 Snyder, V.A., Vázquez, M.A., 2005. STRUCTURE, in: *Encyclopedia of Soils in the*
950 *Environment*. Elsevier, pp. 54–68. [https://doi.org/10.1016/B0-12-348530-](https://doi.org/10.1016/B0-12-348530-4/00533-6)
951 [4/00533-6](https://doi.org/10.1016/B0-12-348530-4/00533-6)

952 Testoni, S.A., de Almeida, J.A., da Silva, L., Andrade, G.R.P., 2017. Clay mineralogy of
953 Brazilian oxisols with shrinkage properties. *Rev. Bras. Cienc. do Solo* 41, 1–16.
954 <https://doi.org/10.1590/18069657rbcs20160487>

955 Tiecher, T., Caner, L., Minella, J.P.G., Evrard, O., Mondamert, L., Labanowski, J.,
956 Rheinheimer, D. dos S., 2017. Tracing Sediment Sources Using Mid-infrared
957 Spectroscopy in Arvorezinha Catchment, Southern Brazil. *L. Degrad. Dev.* 28, 1603–
958 1614. <https://doi.org/10.1002/ldr.2690>

959 Tiecher, T., Caner, L., Minella, J.P.G., Santos, D.R. dos, 2015. Combining visible-based-
960 color parameters and geochemical tracers to improve sediment source
961 discrimination and apportionment. *Sci. Total Environ.* 527–528, 135–149.
962 <https://doi.org/10.1016/j.scitotenv.2015.04.103>

963 Tiecher, T., Minella, J.P.G., Evrard, O., Caner, L., Merten, G.H., Capoane, V., Didoné, E.J., dos
964 Santos, D.R., 2018. Fingerprinting sediment sources in a large agricultural
965 catchment under no-tillage in Southern Brazil (Conceição River). *L. Degrad. Dev.* 29,
966 939–951. <https://doi.org/10.1002/ldr.2917>

967 Tiecher, T., Ramon, R., Laceby, J.P., Evrard, O., Minella, J.P.G., 2019. Potential of

968 phosphorus fractions to trace sediment sources in a rural catchment of Southern
969 Brazil: Comparison with the conventional approach based on elemental
970 geochemistry. *Geoderma* 337, 1067–1076.
971 <https://doi.org/10.1016/j.geoderma.2018.11.011>

972 Tornquist, C.G., Mielniczuk, J., Cerri, C.E.P., 2009. Modeling soil organic carbon dynamics
973 in Oxisols of Ibirubá (Brazil) with the Century Model. *Soil Tillage Res.* 105, 33–43.
974 <https://doi.org/10.1016/j.still.2009.05.005>

975 Torres Astorga, R., de los Santos Villalobos, S., Velasco, H., Domínguez-Quintero, O.,
976 Pereira Cardoso, R., Meigikos dos Anjos, R., Diawara, Y., Dercon, G., Mabit, L., 2018.
977 Exploring innovative techniques for identifying geochemical elements as
978 fingerprints of sediment sources in an agricultural catchment of Argentina affected
979 by soil erosion. *Environ. Sci. Pollut. Res.* 25, 20868–20879.
980 <https://doi.org/10.1007/s11356-018-2154-4>

981 Uber, M., Legout, C., Nord, G., Crouzet, C., Demory, F., Poulénard, J., 2019. Comparing
982 alternative tracing measurements and mixing models to fingerprint suspended
983 sediment sources in a mesoscale Mediterranean catchment.

984 van der Waal, B., Rowntree, K., Pulley, S., 2015. Flood bench chronology and sediment
985 source tracing in the upper Thina catchment, South Africa: the role of transformed
986 landscape connectivity. *J. Soils Sediments* 15, 2398–2411.
987 <https://doi.org/10.1007/s11368-015-1185-4>

988 Viscarra Rossel, R.A., Minasny, B., Roudier, P., McBratney, A.B.B., 2006. Colour space
989 models for soil science. *Geoderma* 133, 320–337.
990 <https://doi.org/10.1016/j.geoderma.2005.07.017>

991 Walkley, A., Black, I.A., 1934. An examination of the Degtjareff Method for determining
992 soil organic matter, and a proposed modification of the chromic acid titration
993 method. *Soil Sci.* 37, 29–38. <https://doi.org/10.1097/00010694-193401000->

994 00003

995 Walling, D.E., 2013. The evolution of sediment source fingerprinting investigations in
996 fluvial systems. *J. Soils Sediments* 13, 1658–1675.
997 <https://doi.org/10.1007/s11368-013-0767-2>

998 Walling, D.E., Peart, M.R., Oldfield, F., Thompson, R., 1979. Suspended sediment sources
999 identified by magnetic measurements. *Nature* 281, 110–113. [https://doi.org/10.1038/281-](https://doi.org/10.1038/2810836a)
1000 [0836/79/370110-04](https://doi.org/10.1038/2810836a)\$01.00

1001 Yu, L., Oldfield, F., 1989. A multivariate mixing model for identifying sediment source
1002 from magnetic measurements. *Quat. Res.* 32, 168–181.
1003 [https://doi.org/10.1016/0033-5894\(89\)90073-2](https://doi.org/10.1016/0033-5894(89)90073-2)
1004

1005 **8 Appendices**

1006 **8.1 Appendix A**

1007 The water discharge (Q) and suspended sediment concentration (SSC) was
1008 monitored at the catchment outlet using automatic equipment's that recorded the water
1009 level and turbidity every 10 min through a pressure water level sensor and a
1010 turbidimeter (Hydrological monitoring station Model SL-2000, Solar®, Brazil),
1011 respectively. The Q was calculated from the water level data using a rating curve. The
1012 turbidity sensor was properly calibrated with SSC measured data obtained from
1013 samples of the water and sediment mixture collected during rainfall-runoff events and
1014 in a daily based schedule used for determination of SSC in the laboratory. In the Figure
1015 A1 shows the Q and SSC data measured with the automatic equipment's are presented.
1016 The period covered by each time integrated sediment samples (TISS) and the date that
1017 fine bed sediment samples (FBS) were collected (Table 1) are illustrated in the Figure
1018 A1. The first TISS (S-9) was installed after the harvesting of the summer crop season of
1019 2011/2012, and the sample collected before to start the following summer crop season,
1020 having a sample which represents the winter period which had less intense rainfall. The
1021 second TISS sample (S-10), represents the period in which the soil is more susceptible
1022 to erosion processes due to the soil preparation and sowing process, which occurs
1023 together with the period of heavier rainfall (September to November). The third
1024 sampling period (S-11) represents the period in which the summer crops are established
1025 and the soil is more protected by the summer crops.

1026 **8.2 Appendix B**

1027 Twenty-four colour parameters were calculated from the ultraviolet-visible
1028 spectra following the colorimetric models described in detail by Viscarra Rossel et al.

1029 (2006), which are based on the Munsell HVC, RGB, the decorrelation of RGB data,
1030 CIELAB and CIELUV Cartesian coordinate systems, three parameters from the HunterLab
1031 colour space model and two indices (coloration – CI and saturation index – SI). First, the
1032 colour coefficients XYZ based on the colour-matching functions defined by the
1033 International Commission on Illumination - CIE (CIE, 1931) were calculated, where X
1034 and Z are the virtual components of the primary spectra and Y represents the
1035 brightness. The XYZ tristimulus were standardised with values corresponding to the
1036 Standard Illuminant D65 white point for 10 Degree Standard Observer ($X = 94.8110$; $Y =$
1037 100.00 ; $Z = 107.304$), then transformed into the Munsel HVC, RGB, CIELAB and CIELUV
1038 Cartesian coordinate systems using the equations from CIE (1978). Three parameters
1039 from the HunterLab (HunterLab, 2015) colour space model, and two indices (coloration
1040 - CI and saturation index - SI) (Pulley et al., 2018) were calculated as well. In total, 27
1041 colour metric parameters were derived from the spectra of potential source and
1042 sediment samples (L , L^* , a , a^* , b , b^* , C^* , h , RI , x , y , z , u^* , v^* , u' , v' , Hvc , hVc , hVc , R , G , B ,
1043 $HRGB$, $IRGB$, $SRGB$, CI and SI).

1044 Three other parameters were calculated from the second derivative curves of
1045 remission functions in the visible range of soil and sediment samples, which displayed
1046 three major absorption bands at short wavelengths commonly attributed to Fe-oxides
1047 (Caner et al., 2011; Fritsch et al., 2005; Kosmas et al., 1984; Scheinost et al., 1998). The
1048 first band ($A1$, ~ 430 nm) corresponds to the single electron transition of goethite (Gt),
1049 whereas the two others correspond to the electron pair transition for goethite ($A2$,
1050 ~ 480 nm) and for hematite (Hm) ($A3$, ~ 520 nm), respectively (Figure B1). The band
1051 intensity is estimated from the amplitude between a minimum and the nearby
1052 maximum at its lower energy side. The amplitudes of the three bands ($A1$, $A2$ and $A3$)
1053 are positively correlated with the contents of Gt and Hm (Fritsch et al., 2005). $A1$ and $A3$

1054 are commonly used to assess the content of Gt and Hm, respectively, and the relative
1055 proportions of hematite in Fe oxides (Hr) are estimated by applying the equation Hr
1056 $(\%) = Hm/(Hm+Gt)$. The band intensities were measured from the amplitude between
1057 each band minimum and its nearby maximum at higher wavelength.
1058

Figure 1
[Click here to download high resolution image](#)

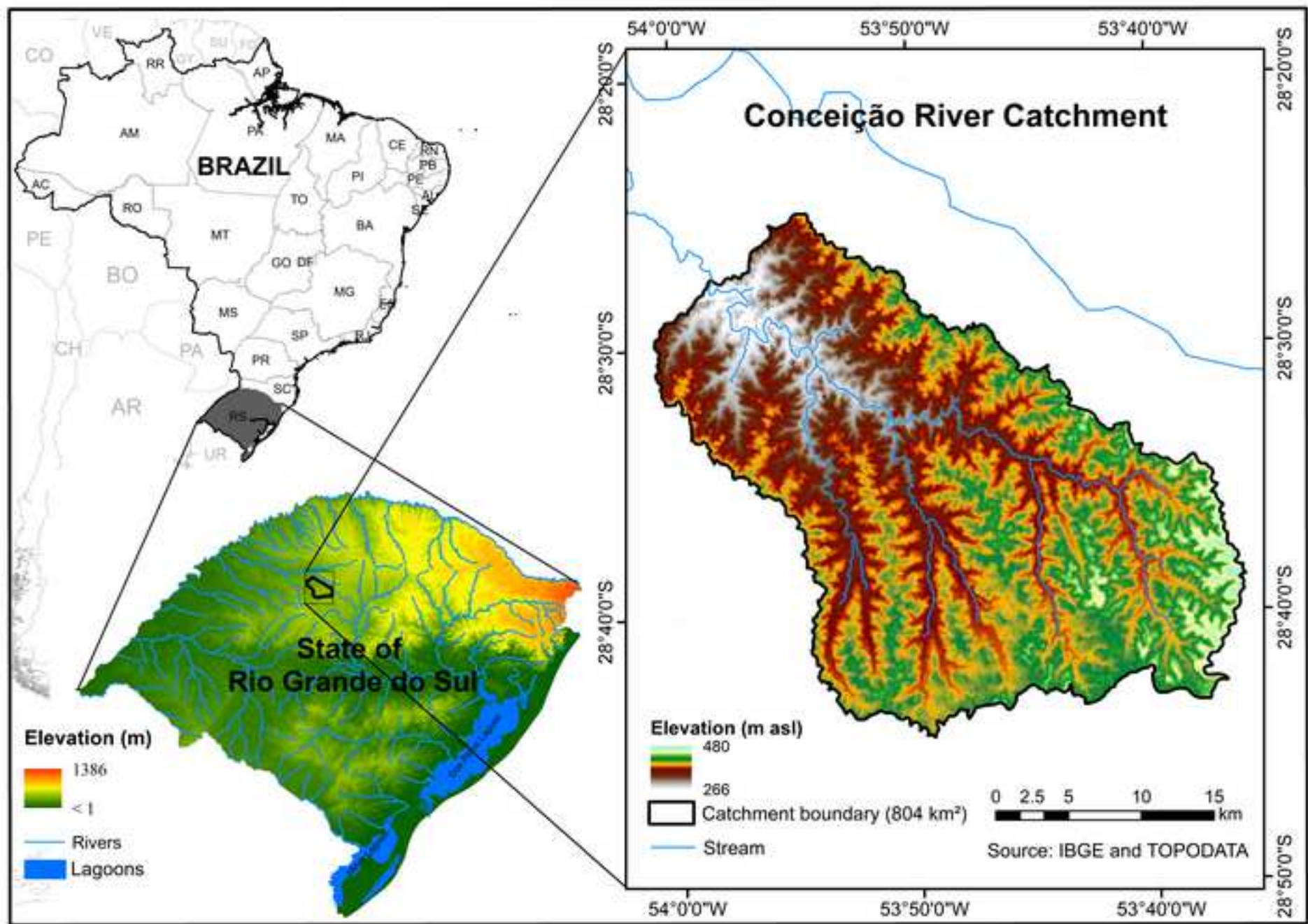


Figure 2

[Click here to download high resolution image](#)

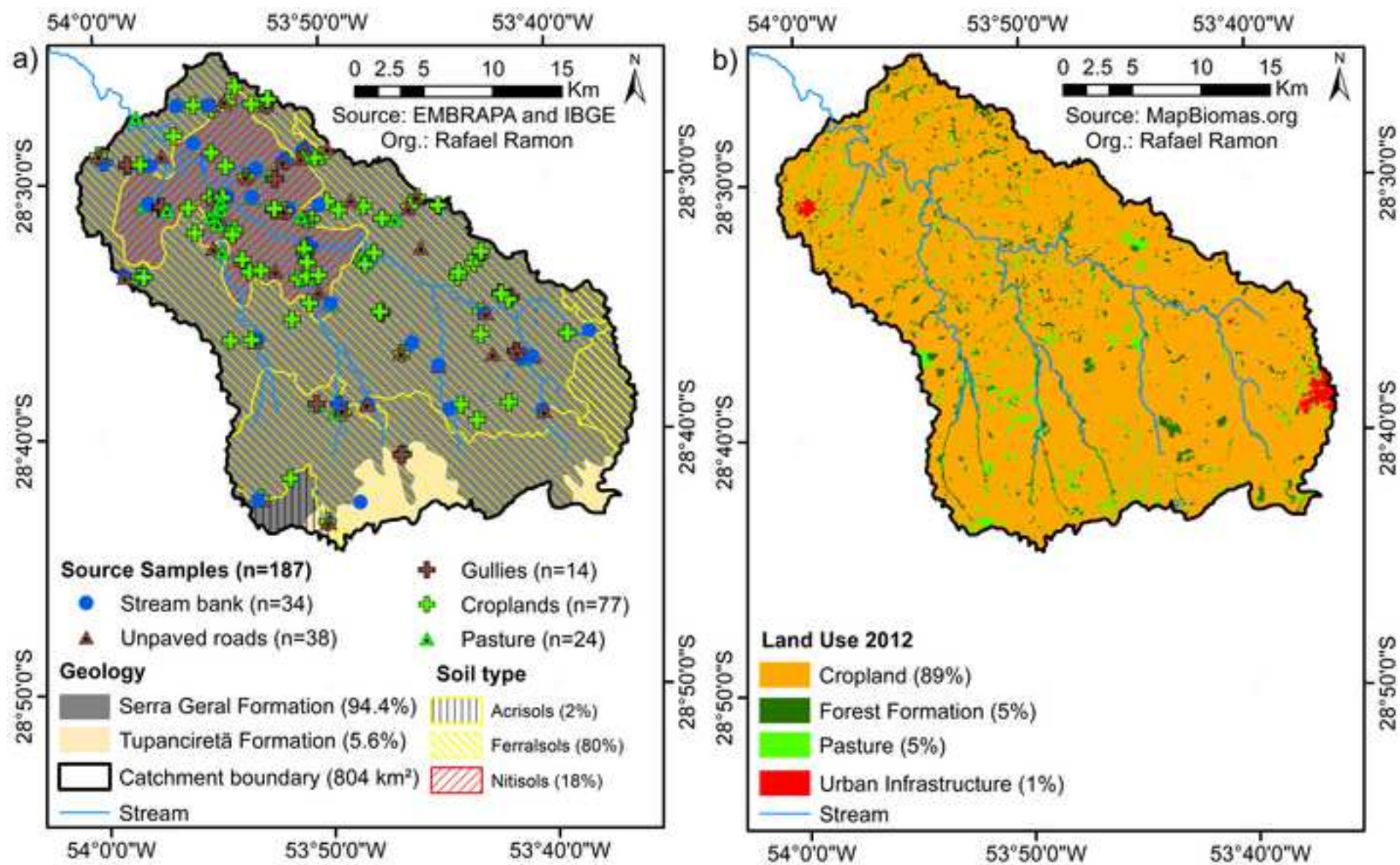


Figure 4
[Click here to download high resolution image](#)

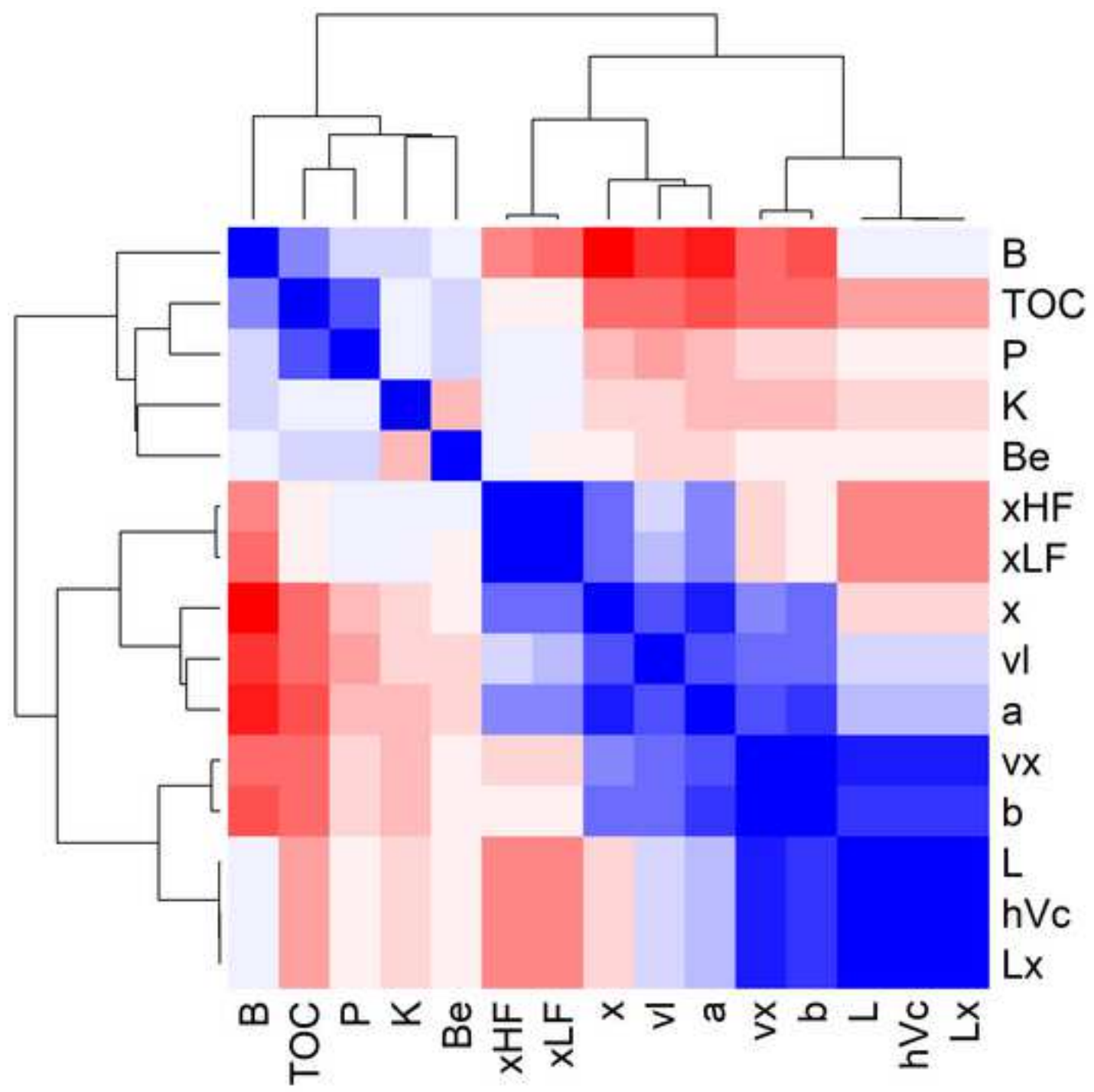


Figure 5
[Click here to download high resolution image](#)

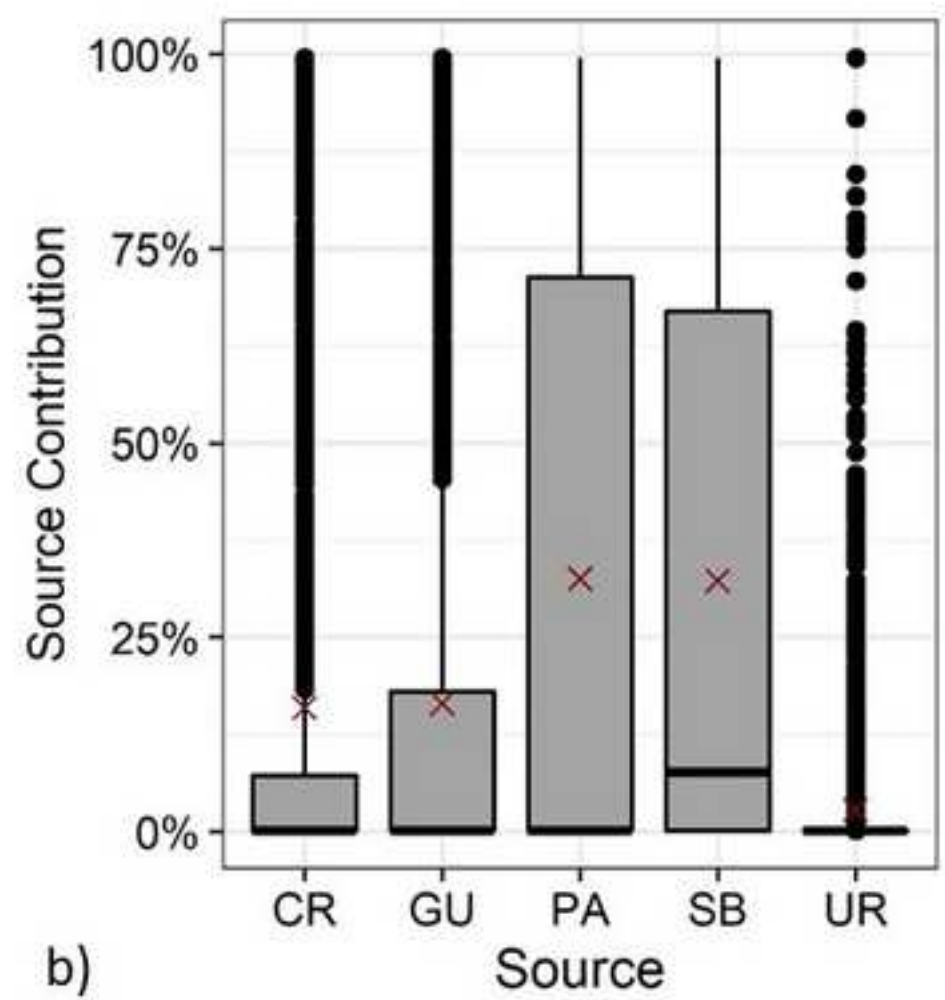
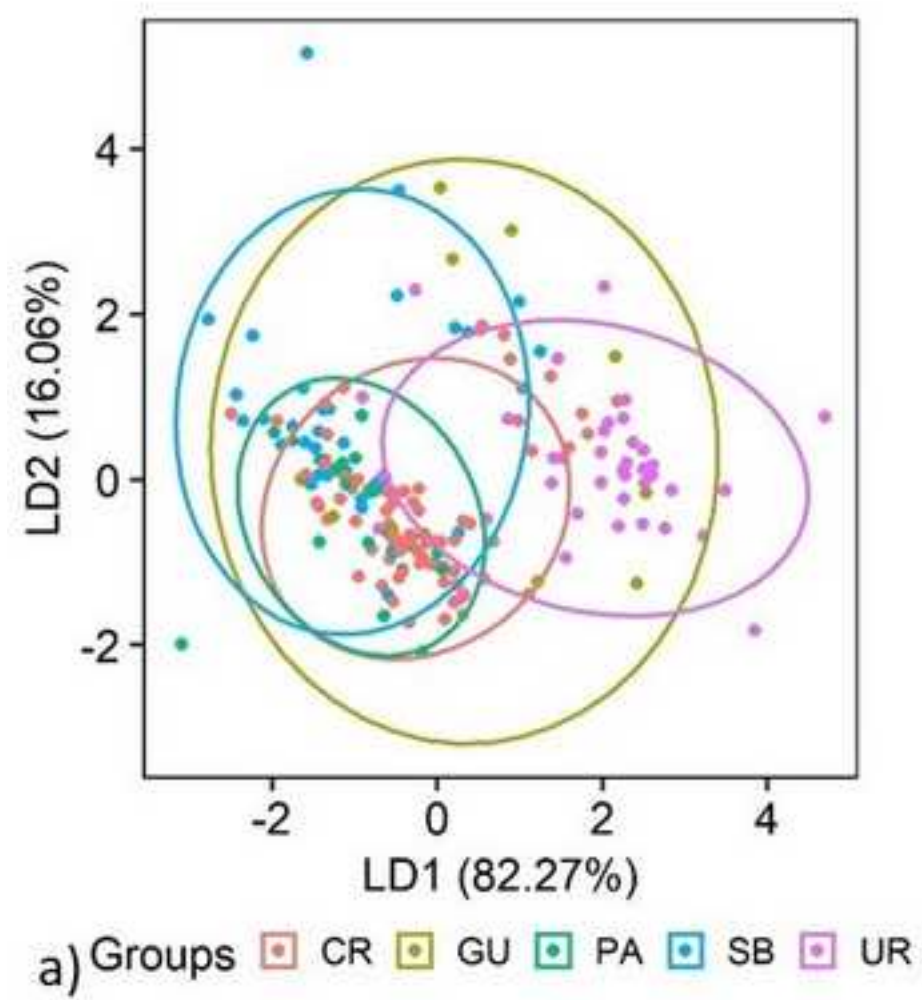
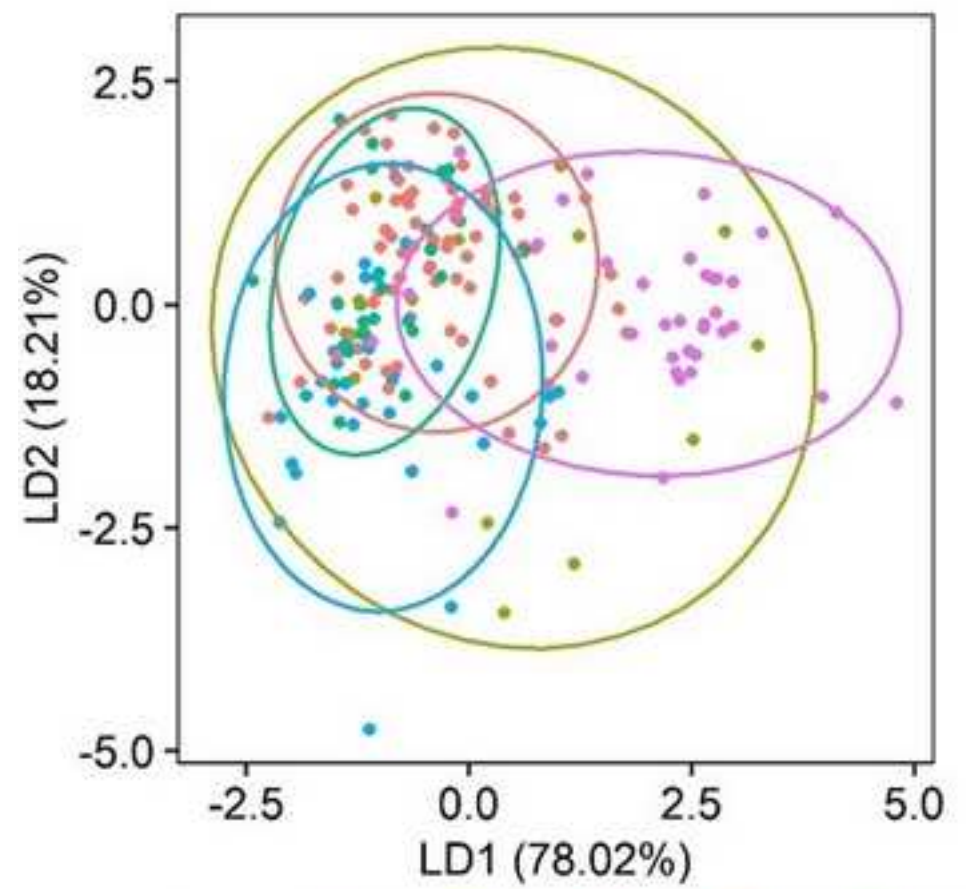
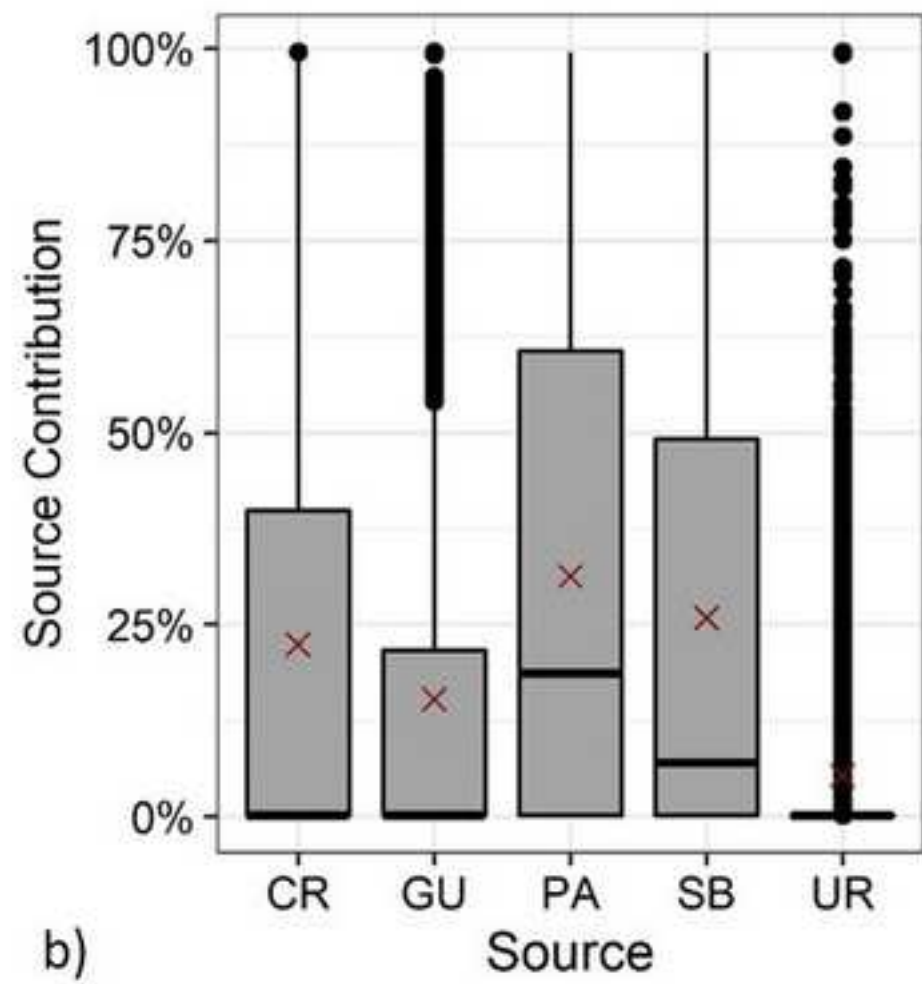


Figure 6
[Click here to download high resolution image](#)

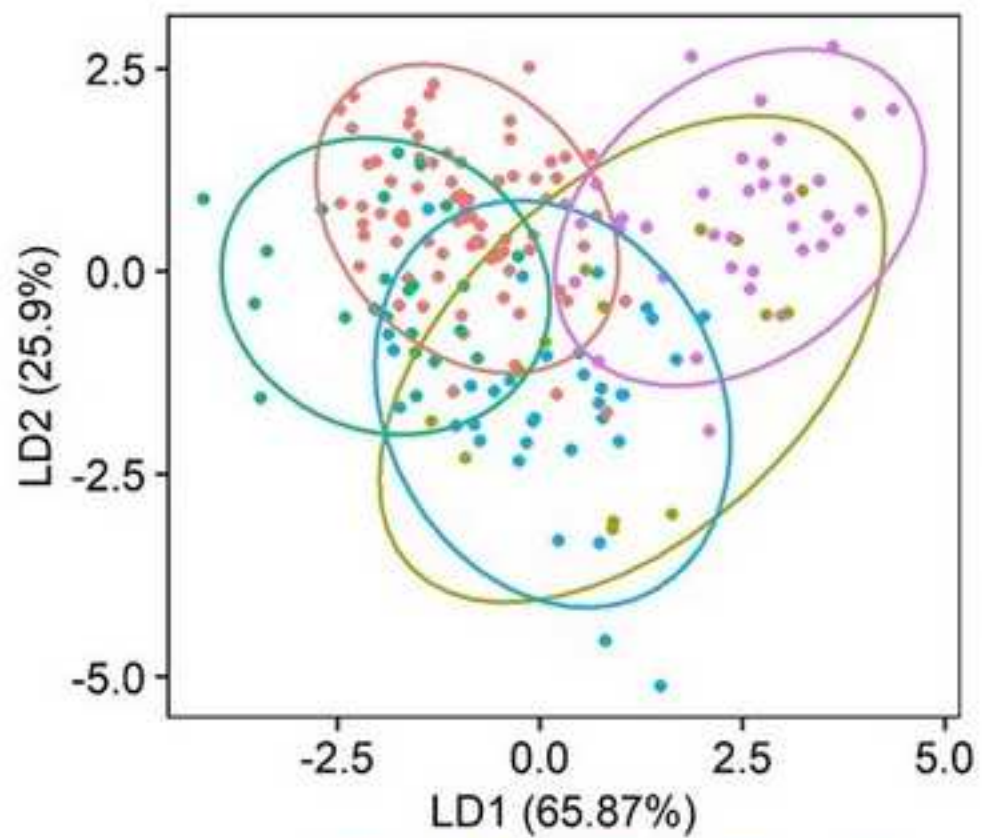


a) Groups ■ CR ■ GU ■ PA ■ SB ■ UR

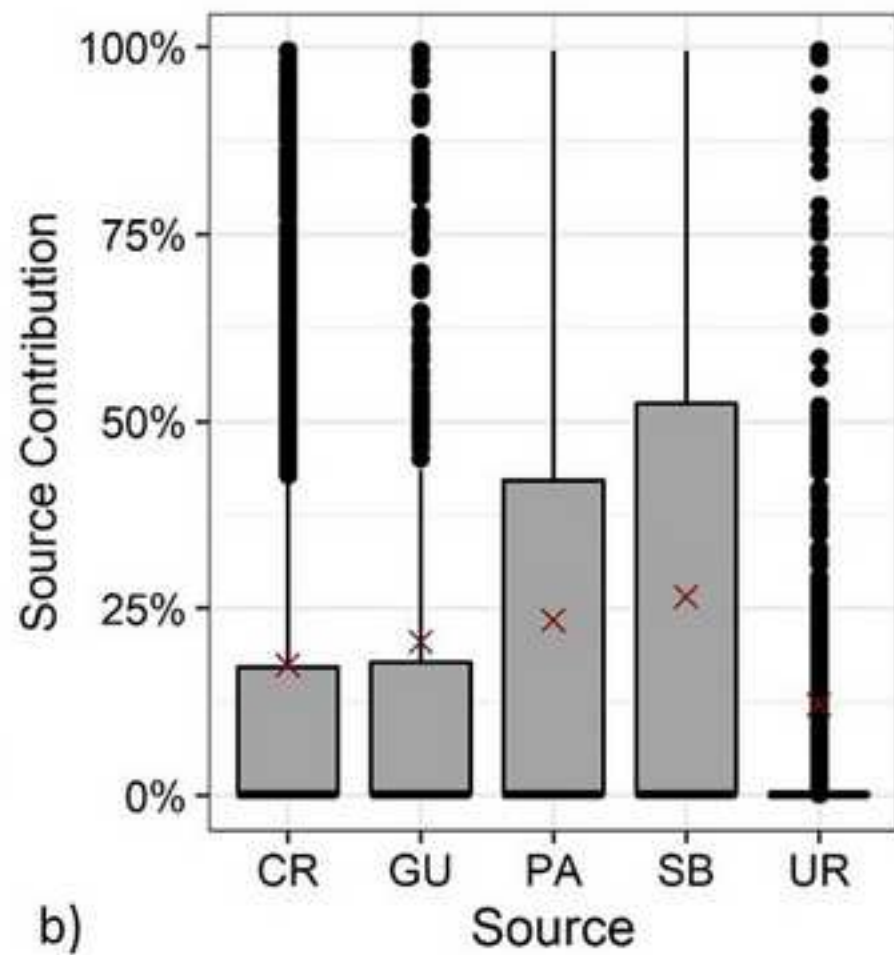


b)

Figure 7
[Click here to download high resolution image](#)

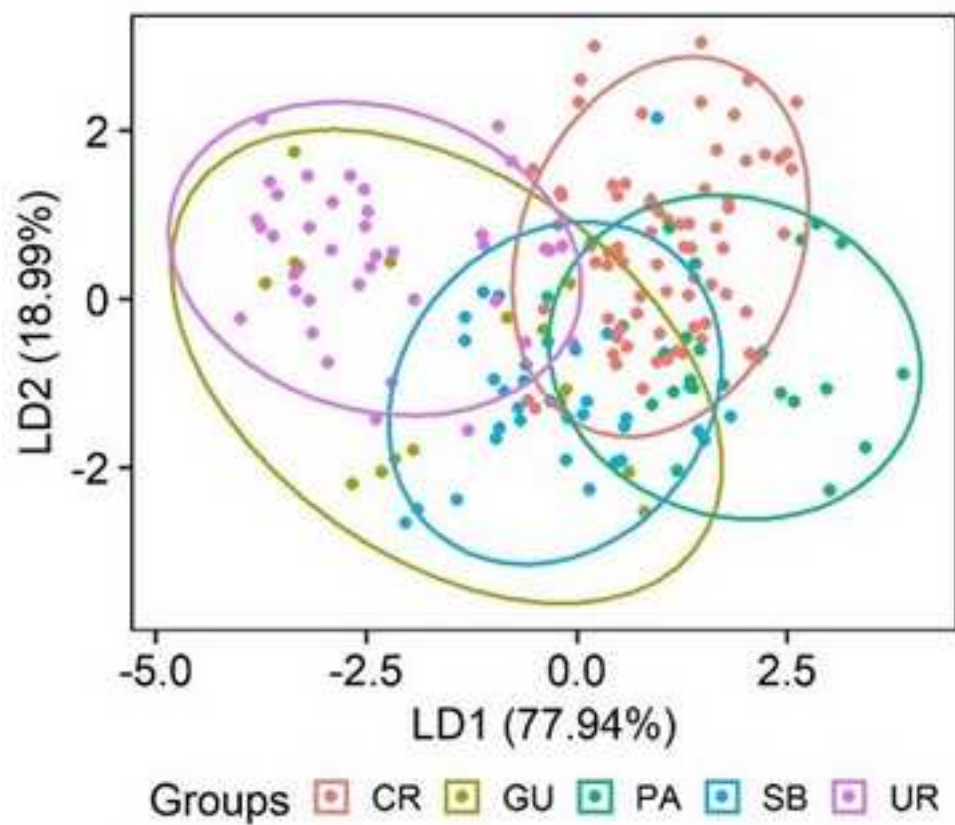


a) Groups ■ CR ■ GU ■ PA ■ SB ■ UR

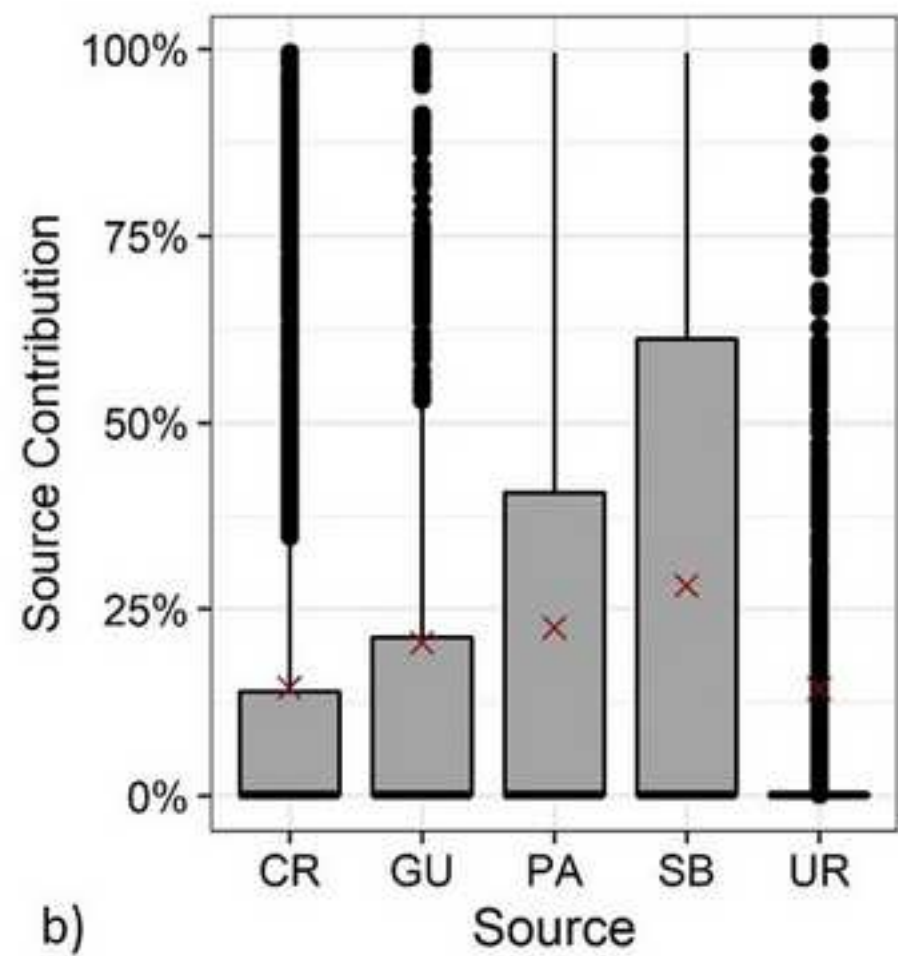


b)

Figure 8
[Click here to download high resolution image](#)



a)



b)

Figure 9

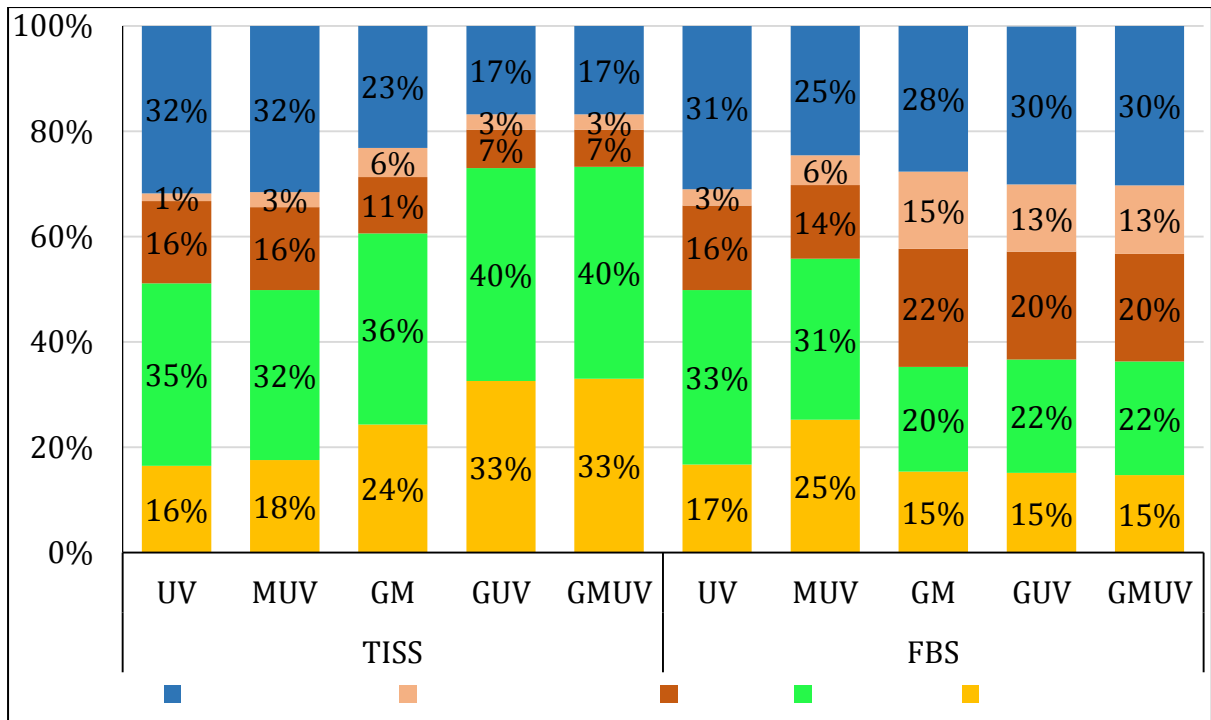


Figure A1

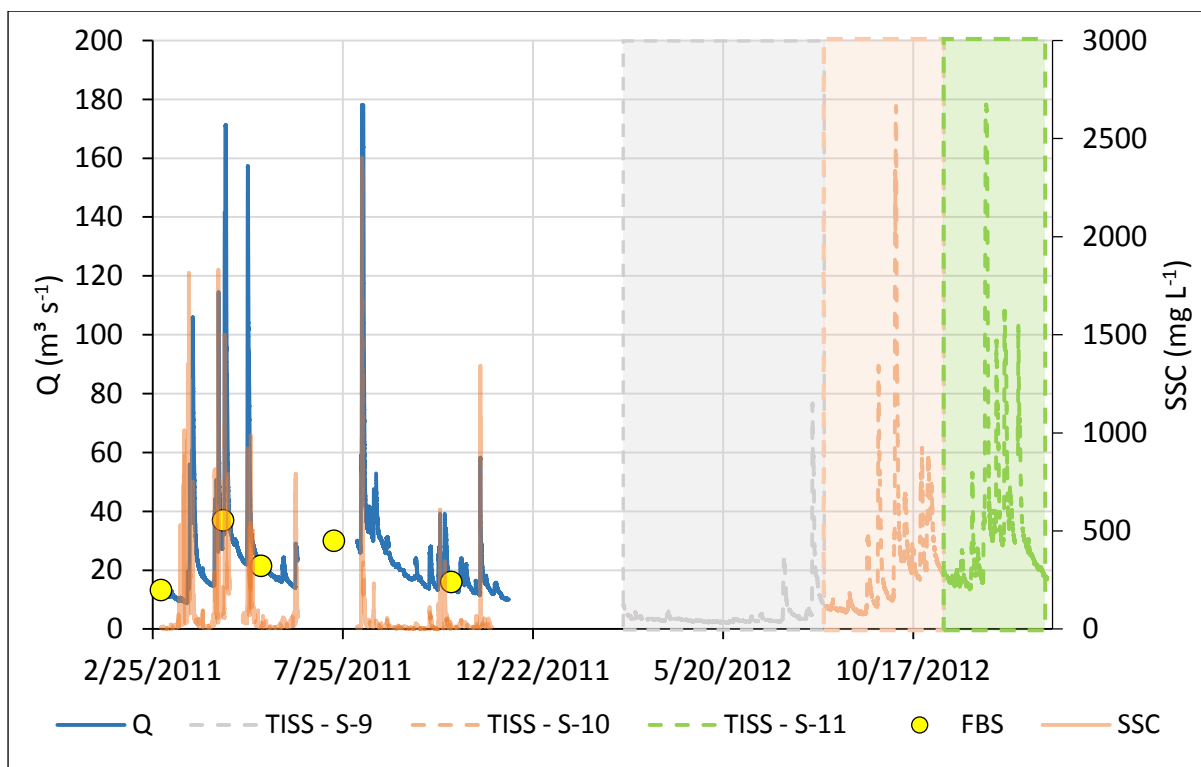
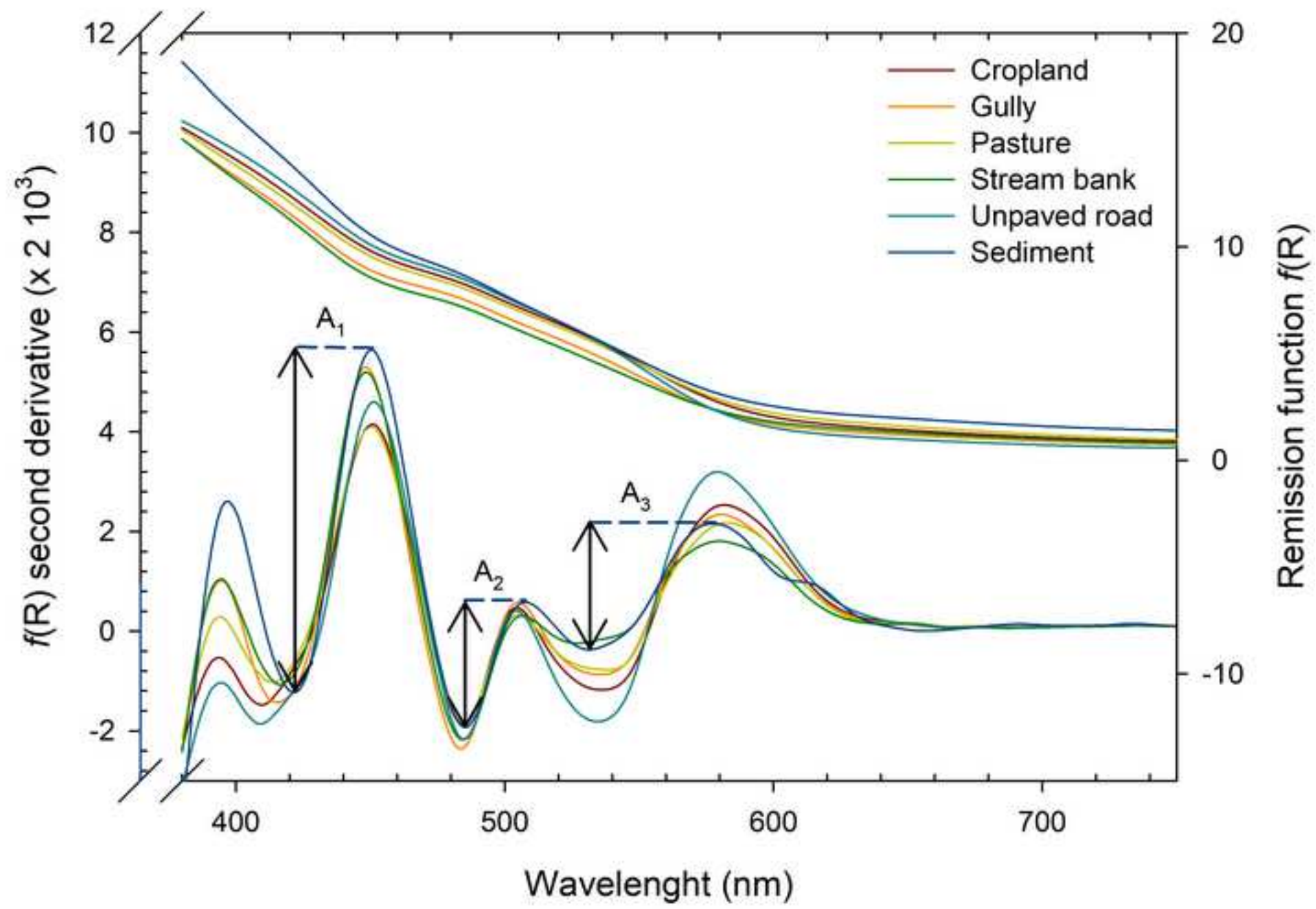


Figure B1
[Click here to download high resolution image](#)



1 **Figure captions**

2 Figure 1. Location of the Conceição River catchment in Southern Brazil and
3 digital elevation model.

4 Figure 2. Lithological formations, soil types and source sample location (a); and
5 land use map for the year 2012 (b).

6 Figure 3. Correlation plot between variables that were approved in the
7 conservativeness test and KW H test. The representation of the symbols “ * ” and “ ’ ”
8 used to differentiate the colour parameters was replaced by the letters “x” and “l” in the
9 figure. xHF and xLF correspond to the magnetic parameters \square_{HF} and \square_{LF} , respectively.

10 Figure 4. Heat map and dendrogram of the variables that were approved in the
11 conservativeness test and KW H test. The representation of the symbols “ * ” and “ ’ ”
12 used to differentiate the colour parameters was replaced by the letters “x” and “l” in the
13 figure. xHF and xLF correspond to the magnetic parameters \square_{HF} and \square_{LF} , respectively.

14 Figure 5. Approach considering only UV-VIS derived parameters – UV. a) Source
15 reclassification by the LDA using the selected variables. b) Box plot with the source
16 contributions. The red cross point represents the mean, the horizontal line inside the
17 box represents the median, the lower and upper edges of the box represent the 25th
18 and 75th percentiles, whiskers represent the 10th and 90th percentiles, and circles
19 represent values greater than the 90th percentile.

20 Figure 6. Approach considering the combination of UV and magnetic – MUV. a)
21 Source reclassification by the LDA using the selected variables. b) Box plot with the
22 source contribution. The red cross point represents the mean, the horizontal line inside
23 the box represents the median, the lower and upper edges of the box represent the 25th

24 and 75th percentiles, whiskers represent the 10th and 90th percentiles, and circles
25 represent values greater than the 90th percentile.

26 Figure 7. Approach considering the combination of GEO and UV parameters –
27 GUV. a) Source reclassification by the LDA using the selected variables. b) Box plot with
28 the source contribution. The red cross point represents the mean, the horizontal line
29 inside the box represents the median, the lower and upper edges of the box represent
30 the 25th and 75th percentiles, whiskers represent the 10th and 90th percentiles, and
31 circles represent values greater than the 90th percentile.

32 Figure 8. Approach considering the combination of geochemical and magnetic
33 parameters – GM. a) Source reclassification by the LDA using the selected variables. b)
34 Box plot with the source contribution. The red cross point represents the mean, the
35 horizontal line inside the box represents the median, the lower and upper edges of the
36 box represent the 25th and 75th percentiles, whiskers represent the 10th and 90th
37 percentiles, and circles represent values greater than the 90th percentile.

38 Figure 9. Mean contributions of each sediment source for the two types of
39 sediment sampling strategies (TISS and FBS) and following the five approaches relying
40 on different tracer combinations.

41 Figure A1. Water discharge (Q) and suspended sediment concentration (SSC)
42 during the monitored period, sampling period of time integrated suspended sediment
43 sampler (TISS) and sampling time of fine bed sediment samples (FBS).

44 Figure B1. Second-derivative spectra of the remission function $f(R)$ from visible
45 diffuse reflectance spectroscopy showing the absorption bands (minima) of Fe-oxides in
46 each landuse and sediment samples mean spectra.

1 Table 1. Sediment samples and their respective period of sampling.

ID	Sample Type*	Collection period
S-1	FBS	02/03/2011
S-2	FBS	21/04/2011
S-3	FBS	21/05/2011
S-4	FBS	18/07/2011
S-5	FBS	18/10/2011
S-6	FBS	02/02/2012
S-7	FBS	24/03/2012
S-8	FBS	10/11/2012
S-9	TISS	02/03/2012 - 09/08/2012
S-10	TISS	17/08/2012 - 10/11/2012
S-11	TISS	10/11/2012 - 30/01/2013

2 *FBS – fine bed sediments and TISS – time integrated sediment samples.

1 Table 2. Tracers removed by the conservative test.

Classical range test	IQR Approach
Co, V, Na, Ti, TOC, K, hvC	Al, Ba, Ca, Co, Cr, Cu, La, Li, Mg, Mn, Na, Ni, Sr, Ti, V, Zn, A1, A2, A3, a*, b*, Cl, C*, G, h, HRGB, hvC, Hvc, IRGB, R, RI, SI, SRGB, u', u*, y, z

2

Table 3[Click here to download Table: Table 3.docx](#)

1 Table 3. Selected tracers by the LDA for each tracer combination and the
2 corresponding percentage of samples correctly classified (SCC).

Tracer combination	Tracers selected	% SCC
GEO	TOC, P, K	68.4%
UV	a, v*, v', b	59.4%
MUV	a, v*, v', b, \square_{HF} , \square_{LF}	60.4%
GUV	TOC, K, P, a, v*, b, L, L*	73.3%
GM	TOC, K, P, \square_{HF} , \square_{LF}	74.3%
GMUV	TOC, K, P, a, v*, b, L, L*	73.3%

3 G - geochemical tracers; UV - UV-VIS derived parameters; M - magnetic variables; SCC - Samples correctly
4 classified.

1 Table 4. Magnetic, geochemical and UV-VIS derived parameters concentrations in the potential sources and in sediment of the
 2 Conceição catchment, and results of the mean test.

Fingerprint property	Cropland	Pastures	Unpaved Road	Stream Banks	Gullies	Sources		Sediments	KW	
	Mean ± SD	Max	Min	Mean ± SD	p value	H value				
n =	77	24	38	34	14	187		11		
□LF (10 ⁻⁶ m ³ kg ⁻¹)	20.1 ± 8	15 ± 7.4	22 ± 8.7	11 ± 5.6	15.3 ± 9.3	42.7	1.7	14 ± 3	< 0.001	38.6
□HF (10 ⁻⁶ m ³ kg ⁻¹)	18.4 ± 7.1	13.9 ± 6.8	19.4 ± 7.5	10.3 ± 5.2	13.7 ± 8	38.0	1.5	13.3 ± 3.1	< 0.001	36.7
TOC (g kg ⁻¹)	22 ± 4.6	25.9 ± 4.8	7.4 ± 4.6	15.7 ± 5.2	10.5 ± 5.9	36.3	1.5	22.4 ± 8.1	< 0.001	116.2
Ba (mg kg ⁻¹)	200.2 ± 84.6	209.7 ± 73.6	131.1 ± 79.4	215.1 ± 56.1	153.2 ± 72.2	500.4	46.1	261.9 ± 38.1	< 0.001	34.5
Be (mg kg ⁻¹)	3.7 ± 0.6	3.6 ± 0.7	3.5 ± 0.6	4 ± 0.6	3.5 ± 0.5	5.5	1.9	3.5 ± 0.6	0.010	13.2
Co (mg kg ⁻¹)	47 ± 21.6	53.3 ± 20.6	28.1 ± 18.8	59.6 ± 20.6	41.4 ± 30.5	118.8	2.6	88.5 ± 18.4	< 0.001	37.1
Cr (mg kg ⁻¹)	76.1 ± 19.1	77.8 ± 18.9	69.7 ± 14.5	79.8 ± 12.4	68.4 ± 26.3	146.4	39.4	88.4 ± 6.3	0.005	15.0
Cu (mg kg ⁻¹)	325.3 ± 66.8	306.3 ± 60.9	318.2 ± 73.1	335.2 ± 61.4	337.1 ± 77.5	568.2	139.3	303 ± 34	0.233	5.6
La (mg kg ⁻¹)	34.8 ± 10.1	31.8 ± 7.1	33.1 ± 10	37.6 ± 8.4	39.9 ± 7.5	66.8	15.8	30.6 ± 2.7	0.019	11.8
Li (mg kg ⁻¹)	56 ± 19.4	48.8 ± 22.2	73.1 ± 25.4	51.2 ± 12.4	63.2 ± 30.4	143.5	21.2	32.8 ± 3.5	< 0.001	24.4
Ni (mg kg ⁻¹)	50.1 ± 16.1	48.9 ± 12.8	53.3 ± 20.2	47.8 ± 11.9	41.7 ± 9.6	122.8	21.3	52.4 ± 2.3	0.240	5.5
Sr (mg kg ⁻¹)	23.9 ± 13	26.1 ± 11.8	13.7 ± 9.2	25.4 ± 8.6	22.4 ± 12.7	84.0	4.4	35 ± 5	< 0.001	55.2
V (mg kg ⁻¹)	365.3 ± 60.2	400.4 ± 70.4	299.7 ± 59.3	381.5 ± 60.4	309.5 ± 58.9	581.4	207.7	561.1 ± 87.5	< 0.001	48.9
Zn (mg kg ⁻¹)	13.8 ± 3.5	14.4 ± 3.5	12.2 ± 2.2	15.3 ± 3	11.9 ± 2.2	33.4	7.2	16.6 ± 2.8	< 0.001	25.7
Al (mg kg ⁻¹)	70578 ± 13882.3	59871.4 ± 11790.3	91786.4 ± 13002.7	61249.2 ± 10386.8	80320.9 ± 22155.4	113258.9	40415.3	50738.9 ± 4175.2	< 0.001	69.2
Ca (mg kg ⁻¹)	2140 ± 1204.3	2088.5 ± 1265.8	585.8 ± 904.3	1797.5 ± 838	1004.8 ± 1231	5423.2	0.0	3381 ± 697.6	< 0.001	67.1
Fe (mg kg ⁻¹)	92707.1 ± 12753.9	86542.5 ± 14868.8	89570.8 ± 11534.2	93838.2 ± 16710.6	90124.2 ± 9441.6	134108.4	48476.4	89629.6 ± 8526.4	0.219	5.7
K (mg kg ⁻¹)	928.9 ± 651.6	821.9 ± 679.9	697.1 ± 550.6	462.7 ± 384.7	535.3 ± 456.1	3392.3	79.7	397.5 ± 362	0.002	17.2
Mg (mg kg ⁻¹)	3142.8 ± 1591.8	3307.3 ± 1352.7	2182.8 ± 892.7	2985.9 ± 891	2875.6 ± 1712.4	8466.5	1239.0	3647.2 ± 360.6	< 0.001	26.9
Mn (mg kg ⁻¹)	1889 ± 580.1	2020.7 ± 746.1	1112.5 ± 546.1	2319.8 ± 1018.1	1739.7 ± 1039.4	5405.6	344.8	2880.2 ± 712.3	< 0.001	45.2
Na (mg kg ⁻¹)	77.4 ± 76.4	85.4 ± 71.1	78.2 ± 96.4	80.4 ± 35.8	60.6 ± 37.7	620.3	0.0	160.2 ± 170.7	0.163	6.5
P (mg kg ⁻¹)	486.9 ± 128.1	403.5 ± 66.2	300.8 ± 90.2	343.9 ± 147.7	256.2 ± 69.3	1104.6	59.7	467.7 ± 77.3	< 0.001	85.3
Ti (mg kg ⁻¹)	3091.8 ± 939	4176 ± 1045.5	2332.8 ± 738.8	3360.3 ± 931.3	2432.1 ± 678.6	6950.7	873.6	18662.4 ± 2472.2	< 0.001	49.2

L*	38.9 ± 3.3	38.3 ± 4.5	40.7 ± 4.8	41.2 ± 3.2	40.7 ± 5.7	52.5	23.8	37.1 ± 3.8	0.013	12.6
a*	16.4 ± 2.5	14.5 ± 2.7	21.5 ± 3.1	14.8 ± 2.5	17.3 ± 3.9	28.9	8.1	12.2 ± 1.5	< 0.001	72.1
b*	23.1 ± 2.2	21.6 ± 2.6	27.3 ± 3.2	24 ± 3.2	24.7 ± 4.2	36.7	15.4	21.5 ± 2.4	< 0.001	52.1
C*	28.4 ± 3.1	26.1 ± 3.6	34.7 ± 4.2	28.2 ± 3.8	30.2 ± 5.4	46.7	17.4	24.7 ± 2.8	< 0.001	60.8
h	54.7 ± 2.8	56.5 ± 3	51.9 ± 2.4	58.3 ± 2.9	55.4 ± 4	65.7	48.5	60.4 ± 1.2	< 0.001	69.0
x	0.4 ± 0	0.4 ± 0	0.5 ± 0	0.4 ± 0	0.4 ± 0	0.5	0.4	0.4 ± 0.006	< 0.001	56.1
y	0.4 ± 0	0.4 ± 0	0.4 ± 0	0.4 ± 0	0.4 ± 0	0.4	0.4	0.4 ± 0.005	< 0.001	42.5
z	0.2 ± 0	0.2 ± 0	0.2 ± 0	0.2 ± 0	0.2 ± 0	0.2	0.1	0.2 ± 0.007	< 0.001	54.7
L	32.6 ± 2.9	32.1 ± 3.9	34.2 ± 4.4	34.6 ± 2.9	34.3 ± 5.1	45.4	20.1	31.1 ± 3.3	0.013	12.7
a	12.5 ± 2.1	10.9 ± 2.3	16.9 ± 2.8	11.4 ± 2.1	13.4 ± 3.3	24.9	5.9	9 ± 1.4	< 0.001	69.2
b	12.3 ± 1.3	11.6 ± 1.6	14.2 ± 1.8	13.1 ± 1.7	13.3 ± 2.4	19.9	7.9	11.4 ± 1.5	< 0.001	37.6
u*	33.6 ± 4.8	29.9 ± 5.4	43.5 ± 6.3	32.1 ± 5.1	36 ± 7.8	62.3	17.9	26.4 ± 3.8	< 0.001	65.7
v*	21.8 ± 2.2	20.8 ± 2.8	24.7 ± 3	23.5 ± 3.1	23.5 ± 4.3	34.7	13.9	20.9 ± 2.8	< 0.001	32.8
u'	0.3 ± 0	0.3 ± 0	0.3 ± 0	0.3 ± 0	0.3 ± 0	0.3	0.2	0.3 ± 0	< 0.001	60.8
v'	0.5 ± 0	0.5 ± 0	0.5 ± 0	0.5 ± 0	0.5 ± 0	0.5	0.5	0.51 ± 0	< 0.001	65.4
RI	2.5 ± 1.5	3.5 ± 4.9	2.2 ± 1.2	1.8 ± 1	2.8 ± 4.1	25.8	0.5	3.1 ± 2.2	0.006	14.4
Hvc	163.7 ± 8.6	169.7 ± 9.7	152.3 ± 8.1	172.6 ± 8.1	164.2 ± 12.9	192.3	141.0	178.9 ± 3.3	< 0.001	71.5
hVc	23.4 ± 1.5	23.1 ± 2.1	24.2 ± 2.2	24.5 ± 1.4	24.3 ± 2.6	29.6	16.5	22.6 ± 1.7	0.013	12.7
hVc	30.0 ± 2.6	28.1 ± 3.1	35.2 ± 3.4	29.9 ± 3.0	31.6 ± 4.4	45.7	21.6	26.6 ± 2.6	< 0.001	60.8
R	193.5 ± 12.6	184.7 ± 14.0	216.1 ± 16.5	185.7 ± 12.3	196.8 ± 21.6	238.9	150.4	178.3 ± 4.9	< 0.001	60.2
G	74.8 ± 3.5	77.2 ± 3.6	68.7 ± 4.4	78.5 ± 3.2	74.5 ± 6.0	85.5	62.1	81 ± 1.1	< 0.001	70.2
B	34.2 ± 3.5	36.5 ± 4.1	28.1 ± 4.9	34.7 ± 4.2	32.8 ± 6.3	48.0	21.8	36.2 ± 1.9	< 0.001	53.5
HRGB	19.5 ± 4.1	16.7 ± 4.3	26.7 ± 5.2	15.8 ± 3.7	20.1 ± 6.9	34.1	7.5	13.1 ± 1.3	< 0.001	66.9
IRGB	100.8 ± 1.9	99.5 ± 2.2	104.3 ± 2.5	99.6 ± 1.9	101.3 ± 3.3	107.8	94.2	98.5 ± 0.8	< 0.001	60.2
SRGB	79.7 ± 8.0	74.1 ± 9.0	94.0 ± 10.6	75.5 ± 8.1	82.0 ± 13.8	108.3	51.2	71 ± 3.4	< 0.001	58.8
CI	0.44 ± 0.05	0.41 ± 0.05	0.52 ± 0.05	0.40 ± 0.04	0.45 ± 0.08	0.6	0.3	0.38 ± 0.02	< 0.001	64.7
SI	0.70 ± 0.04	0.67 ± 0.05	0.77 ± 0.05	0.68 ± 0.05	0.71 ± 0.08	0.8	0.5	0.66 ± 0.02	< 0.001	56.6
A1	0.003 ± 0.001	0.003 ± 0.002	0.004 ± 0.001	0.004 ± 0.002	0.004 ± 0.002	0.0	0.0	0.005 ± 0.001	< 0.001	19.9
A2	0.001 ± 0	0.001 ± 0.001	0.001 ± 0.001	0.001 ± 0.001	0.001 ± 0.001	0.0	0.0	0.002 ± 0.001	0.111	7.5
A3	0.002 ± 0.001	0.002 ± 0.001	0.003 ± 0.001	0.001 ± 0.001	0.002 ± 0.002	0.0	0.0	0.003 ± 0.001	< 0.001	51.0

3 SD – Standard Deviation

Table 5[Click here to download Table: Table 5.docx](#)

- 1 Table 5. Mean contribution and mean standard deviation of each source contribution for all target sediment samples and for
 2 individual sediment sampling strategies conducted in the Conceição River catchment.

	Approaches	CR (%)			GU (%)			PA (%)			SB (%)			UR (%)		
		Mean	TISS	FBS	Mean	TISS	FBS	Mean	TISS	FBS	Mean	TISS	FBS	Mean	TISS	FBS
Source contribution	UV	16.6a	16.5b	16.7ab	15.9a	15.6a	16.0a	33.6a	34.7a	33.2a	31.2a	31.8ab	31.0a	2.6b	1.5b	3.1b
	GM	17.8a	24.3ab	15.4b	19.2a	10.7a	22.4a	24.4a	36.3a	19.9b	26.4a	23.2ab	27.7a	12.2a	5.5a	14.7a
	GUV	19.9a	32.5a	15.1b	17.0a	7.3a	20.6a	26.7a	40.5a	21.5ab	26.3a	16.8b	29.9a	10.1a	2.9a	12.8a
	MUV	23.1a	17.6ab	25.2a	14.4a	15.8a	14.0a	31.1a	32.3a	30.6ab	26.4a	31.5a	24.6a	4.9ab	2.9a	5.7ab
	GMUV	19.6a	32.6a	14.8b	17.1a	7.2a	20.8a	26.4a	40.3a	21.2ab	26.6a	17.1ab	30.2a	10.2a	2.8a	13.0a
Standard deviation	UV	31.7	31.8	31.6	29.5	29.2	29.7	38.2	38.6	38.0	36.9	37.2	36.9	9.5	7.5	10.2
	GM	26.7	26.9	26.7	29.7	19.6	33.5	30.9	31.8	30.6	34.5	27.9	37.0	23.9	13.4	27.8
	GUV	28.2	29.4	27.8	28.3	15.5	33.0	31.8	31.2	32.1	34.4	23.7	38.4	22.0	9.0	26.9
	MUV	28.1	29.5	27.6	28.3	15.5	33.1	31.7	31.2	31.8	34.5	23.9	38.5	22.0	8.6	27.0
	GMUV	30.4	27.4	31.5	24.6	26.1	24.1	32.9	34.1	32.5	31.3	34.0	30.2	12.3	10.1	13.1

- 3 *Means followed by the same letter in the columns do not differ statistically by the Kruskal-Wallis H-test at $p < 0.05$. TISS = Time
 4 Integrated Sediment Sampler (n=3); FBS = Fine bed sediment samples from the river bottom (n=8); CR = Croplands; GU = Gullies, PA =
 5 Pastures; SB = Stream banks; and UR = Unpaved roads.